



NTNU – Trondheim
Norwegian University of
Science and Technology

3D Numerical Modelling of Hydropeaking Scenarios in Norwegian Regulated Rivers

Øyvind Pedersen

Civil and Environmental Engineering

Submission date: June 2012

Supervisor: Nils Rüther, IVM

Norwegian University of Science and Technology
Department of Hydraulic and Environmental Engineering

Assignment

Hydropower peaking has become extremely popular among the energy suppliers when it comes to production of energy from an electrical hydropower plant. Electricity is produced in times of the day where the demand is high. Since these periods are short and frequently reoccurring, it can happen that the water level in the river is changing heavily during one day. The effects of this frequent changes has been studied recently, however many effects yet remain unknown, e.g. the effects of the frequent flow changes on the river bed.

NTNU and SINTEF is currently cooperating on the CEDREN project EnviPEAK, studying hydro power peaking effects in the river Surna. The goal of this master-thesis will therefore be to assess the possibilities for using computational fluid dynamics (CFD) for predicting hydraulic conditions in Norwegian regulated rivers. Two different software-packages will be compared. The software used will include the in-house NTNU developed, non-commercial package SSIIM, and the commercial package STAR CCM+ developed by CD-Adapco. Some work on a SSIIM model has already been done by the candidate in relation to the course TVM4520 "Vassdragsteknikk" during the autumn 2011. This includes a free-surface simulation in SSIIM as well as topographic, hydrologic and sediment data from the river Surna near Svean. This work will be used as a basis for the master thesis. The further model work in SSIIM will be done by the supervisor for this thesis Associate professor Nils R  ther, while modeling in Star CCM+ will be done as part of the thesis. Two rivers will be modeled, Surna and Lundesokna. Lundesokna will be modeled with Star CCM+.

The master thesis will address the following points:

- How grids can be made for the two rivers in Star CCM+
- How steady flow free surface simulations can be run for both rivers in Star CCM+
- How unsteady simulations can be run for both rivers in Star CCM+
- As Surna is not currently operated as a hydro-peaking system, a hypothetical hydro-peaking scenario will be developed.

- In Lundesokna, video footage from a full-scale hydropeaking experiment will be used to make a scenario.
- The models and results from the SSIIM and Star CCM+ simulations in Surna will be compared and discussed.
- The results from the Star CCM+ simulations in Lundesokna will be compared to field data and discussed.

As a bi-product of the thesis, a conference paper on the comparison of the two packages will be delivered as a contribution to the River Flow 2012 conference in Costa Rica. The paper will be co-authored with Associate professor Nils R  ther who will also be the main supervisor for the thesis.

Preface

During my last two semesters as a MSc student at the Department of Hydraulic and Environmental Engineering I have had the pleasure of being involved in the exciting research carried out in connection to the EnviPEAK project at CEDREN (the Centre for Environmental Design of Renewable Energy). CEDREN is a joint operation by SINTEF, NINA and NTNU, financed by the Research Council of Norway and several energy companies. The aim of the EnviPEAK project is to investigate the environmental impact of the rapid changes in water levels and flow patterns that can be induced by hydro-peaking operation of Norwegian power plants.

I was first involved in the project in connection to my work as a lab-assistant, where I worked on the collection of field data and sieving analysis of sediment probes. At the time I also developed an interest for the field of 3D CFD modeling through Professor Nils Reidar Bø Olsen's excellent course "Numerical hydraulics" taught at NTNU. For my 7th semester project work it was therefore only natural to work with CFD modeling in connection to the EnviPEAK project. My project work involved the process of collecting and treating field data as well as using the data to make a CFD model in the free-ware code SSIIM which is the work of Professor Olsen. This master's thesis extends the project by modeling two rivers in the commercial CFD code Star CCM+.

Originally, the objective of this thesis was only to model the river Surna. It was however discovered that the necessary cell count to get satisfactory results was too high to be able to run with the available computational resources. It was therefore decided to discontinue efforts on Surna and concentrate on modeling the smaller river Lundesokna. A paper for the IAHR-APD 2012 conference was written on the experiences from the Surna modeling (Pedersen & R  ther, 2012b). The paper can be found as a digital attachment (Appendix A) but is not a part of this master's thesis.

Acknowledgements

My connection at EnviPEAK and supervisor throughout the project, as well as co-author on the conference paper has been Associate professor Nils R  ther, and I owe him great thanks for his continuous support and for the opportunity to work with the fascinating field of CFD. I also want to thank the brilliant NTNU and SINTEF scientists working with EnviPEAK for all their help supplying field data and digital elevation models. In particular I would like to thank Ph.D candidate Roser Casas-Mullet for supplying invaluable data and support for modeling Lundesokna. I would also like to thank MSc student   smund Hasaas and Ph.D candidate Hanne N  vik for lending me their Matlab-script for treating ADCP-velocity measurements, Samuel Vingerhagen for help and support while I was learning to use Star CCM+, and Sandra Howe at Tecplot for supplying me with free licenses throughout both the project and the master thesis. Finally I would like to extend thanks to Clemence Carnerero, Kirsten Christiansen, Henning Helg  y and Kristine Lilleeng Wall  e for their tireless quality assurance effort.

Abstract

The objective of this master's thesis has been to investigate the capabilities of the CFD packages Star CCM+ and SSIIM to model hydro-peaking scenarios in regulated natural rivers in 3D using a RANS method. Two Norwegian regulated rivers are modeled, Surna and Lundesokna. In Surna, flow fields and bed shear-forces are compared for the Star CCM+ and SSIIM models. In Lundesokna flow fields and water surface elevations from simulations in Star CCM+ are compared to field data at steady flow conditions. For unsteady flow a Star CCM+ simulation are compared to video footage of a hydro-peaking event.

The Surna Star CCM+ numerical model predicts a comparable flow field to SSIIM for both steady and unsteady flow. The magnitudes of velocities and shear-forces, however, deviate. Unphysical velocities and shear forces were found in parts of the cells in the Star CCM+ model. A review of the model shows that the unphysical velocity errors are likely caused by a too coarse grid and problems with the VOF method. Efforts to run simulations on a finer grid were discontinued because of a lack of available computational resources.

Both the Surna numerical models achieved convergent solutions for unsteady flow. However, due to the quasi-unsteady treatment of the flow in SSIIM the SSIIM model is not able to capture wave effects. In consequence the SSIIM model predicts shear-force peaks about 600 seconds earlier than the Star CCM+ model at the outlet. When accounting for this effect the models show similar flow fields but deviating velocity and shear-force magnitudes as for the steady flow.

Comparison to field data show that the Lundesokna Star CCM+ model is able to predict flow fields and water surface elevation with high accuracy for steady flow between $10 \text{ m}^3/\text{s}$ and $20 \text{ m}^3/\text{s}$ discharge. The unsteady flow simulation shows visual resemblance with the video footage, however, field data measurements are required to quantify the accuracy of the numerical model for transient conditions.

Sammendrag

Målet for denne masteroppgaven har vært å undersøke hvor godt egnet CFD-programvaren SSIIM og Star CCM+ er til å modellere hydrauliske effekter i regulerte naturlige elver i 3D ved bruk av en RANS metode. To regulerte elver i Norge blir modellert, Surna og Lundesokna. I Surna sammenliknes simulerte hastighetsfelt og skjærkrefter på elvebunnen i to numeriske modeller i henholdsvis Star CCM+ og SSIIM. I Lundesokna sammenliknes simulerte hastighetsfelt og vannlinjer i Star CCM+ med data målt i felt for stasjonær strømning. For ikke-stasjonær strømning sammenliknes simulerte data med videomateriale fra en effektkjøringstest.

Star CCM+ modellen for Surna produserer sammenliknbare strømningsfelt i forhold til SSIIM modellen. Størrelsen på hastigheter og skjærspenninger er imidlertid avvikende. Tydelig feilaktige hastigheter og skjærspenninger ble observert i deler av cellene i Star CCM+ modellen. Nærmere undersøkelser av modellen antyder at feilene skyldes et for grovt grid og problemer med VOF metoden. Forsøk på å kjøre simuleringer på et finere grid ble ikke gjennomført på grunn av manglende datakraft.

Begge de numeriske modellene for Surna oppnådde løsninger med god konvergens for ikke-stasjonær strømning. På grunn av begrensninger i behandlingen av transiente problemer i SSIIM er SSIIM modellen imidlertid ikke i stand til å simulere effekten av bølger. Dette fører til at maksimale skjærspenninger ved utløp oppnås 600 sekunder tidligere i SSIIM enn i Star CCM+. Når effekten av dette tas i betraktning produserer SSIIM og Star CCM+ modellene sammenliknbare strømningsfelt, men avvikende hastighet og skjærspenningsstørrelser. Dette er tilsvarende som for stasjonær strømning.

Sammenlikning med data målt i felt viser at Star CCM+ modellen for Lundesokna angir hastighetsfelt og vannlinjer med god nøyaktighet for stasjonær strømning mellom 10 og 20 m³/s. For ikke-stasjonær strømning er simuleringen sammenliknbar med videomaterialet, men målinger i felt er nødvendig for å kunne kvantifisere nøyaktigheten av simuleringen.

List of symbols

E	wall function coefficient
f	roughness function
f_p	power-law reduction factor
F	fraction of fluid
g	gravitational acceleration
G	other forces
h	water depth
k	turbulent kinetic energy
k_s	Nikuradse equivalent sand-grain roughness height
L	length scale
p	pressure
P	the production of kinetic energy
Pe	Peclet number
Q	discharge
s	statistical sample
t	time
u_i	instantaneous velocity in direction i
U_i	time-averaged velocity in direction i
u'_i	fluctuating velocity in direction i
u^*	shear velocity
V'	velocity scale

x

x_i	spatial coordinate in direction i
y	normal distance from wall to the wall-cell centroid
z	riverbed elevation
z_s	water surface elevation
Γ	flux coefficient
ε	dissipation of the turbulent kinetic energy
κ	Von Kármán constant
μ	dynamic viscosity
ν	kinematic viscosity
ν_t	eddy-viscosity
ρ	fluid density
τ_{ij}	turbulent stress
ϕ	scalar quantity

List of Abbreviations

ADCP	Acoustic Doppler Current Profiler
CEDREN	Centre for Environmental Design of Renewable Energy
CFD	Computational Fluid Dynamics
DEM	Digital Elevation Model
DES	Detached Eddy Simulation
EnviPEAK	Environmental impacts of hydropeaking
GIS	Geographical Information System
GPS	Global Positioning System
IAHR-APD	The Asia and Pacific Division of the International Association for Hydro-Environment Engineering and Research
LES	Large Eddy Simulation
NINA	Norwegian Institute for Nature Research
NRMSD	Normalized Root-Mean-Square Deviation
NTNU	Norwegian University of Science and Technology
POW	Power-Law Scheme
RANS	Reynolds Averaged Navier-Stokes equations
RMSD	Root-Mean-Square Deviation
SIMPLE	Semi Implicit Method for Pressure Linked Equations
SOU	Second Order Upwind Scheme
SSIIM	Sediment Simulation In water Intakes with Multi-block option
VOF	Volume of Fluid

Table of contents

Assignment	i
Preface.....	iii
Acknowledgements	iv
Abstract	v
Sammendrag	vii
List of symbols	ix
List of Abbreviations	xi
Table of contents.....	xiii
Figures.....	xvii
Tables	xviii
1 Introduction	1
1.1 Background	1
1.2 Focus and limitations	2
1.3 Outline	3
2 Numerical modeling of the Navier-Stokes equations	5
2.1 Introduction	5
2.2 Governing equations.....	5
2.3 Turbulence models	7
2.3.1 Modeling the eddy-viscosity.....	7
2.3.2 The k- ϵ model	8
2.4 Grids.....	10
2.4.1 Grid quality	11
2.5 Discretization of the convective and diffusive terms.....	12
2.5.1 Upwind differencing	13

2.6	Boundary conditions	14
2.6.1	Wall laws.....	14
3	Software.....	17
3.1	Star CCM+	17
3.1.1	Introduction.....	17
3.1.2	Physics models.....	17
3.1.3	Boundaries.....	17
3.1.4	Mesh generation	18
3.1.5	Volume of fluid (VOF) algorithms	21
3.2	SSIIM	23
3.2.1	Introduction.....	23
3.2.2	Physics models.....	23
3.2.3	Adaptive grid approach	24
4	Hardware	25
5	Grid generation method	27
6	Modeling Surna.....	31
6.1	Background	31
6.2	Site description	32
6.3	Hydro-peaking scenario	34
6.4	Data basis.....	35
6.4.1	Bathymetry and digital elevation model	35
6.4.2	Hydrology	36
6.4.3	Sediment data	37
6.5	Calibration of the roughness height	38
6.6	Grids.....	39
6.7	Physics and model assumptions	41
7	Modeling Lundesokna	43
7.1	Background	43
7.2	Site description	44

7.3	Hydro-peaking scenario	45
7.4	Data basis	46
7.4.1	Bathymetry and Digital elevation model	46
7.4.2	Water surface elevation and discharge measurements	47
7.4.3	Velocity measurements	49
7.4.4	Field data from the hydro-peaking event	51
7.4.5	Sediment data	52
7.5	Grid sensitivity tests	53
7.6	Calibration of the model	54
7.7	Characteristics of the final grids	56
7.8	Physics and model assumptions	58
8	Results	61
8.1	Surna	61
8.1.1	Steady flow results	61
8.1.2	Unsteady flow results	65
8.2	Lundesokna	67
8.2.1	Steady flow results	67
8.2.2	Steady flow validation	69
8.2.3	Unsteady flow results	75
9	Discussion	79
9.1	Quality of the digital elevation models	79
9.2	Grid generation	82
9.2.1	Star CCM+ versus SSIIM grid generators	82
9.2.2	Measures to reduce computational time in air-filled cells	82
9.3	Calibration of the roughness height parameter (k_s)	84
9.4	Results for Surna	85
9.4.1	Steady flow	85
9.4.2	Unsteady flow	87
9.4.3	Validation	88

9.5	Results for Lundesokna	88
9.5.1	Steady flow	88
9.5.2	Unsteady flow.....	89
9.6	The width to depth ratio.....	90
10	Conclusion	91
10.1	Recommendations for further work	93
11	Bibliography.....	95
12	Appendixes	99
	Appendix A: List of digital attachments	99
	Hydro-peaking event video footage	99
	Lundesokna unsteady results	99
	Documents.....	99
	Appendix B: Grid sensitivity tests in Lundesokna	100
	Appendix C: Map of the sites	102

Figures

Figure 1: Reynolds averaging.....	6
Figure 2: unstructured 3D grids from Star CCM+ (CD-Adapco, 2011). Left: Mix of hexahedral and polyhedral cells. Right: tetrahedral cells.	10
Figure 3: Arrangement of Control Volumes (Murthy, 2002)	12
Figure 4: Equivalent sand-grain roughness height (k_s) (Labiod, Godillot, & Caussade, 2007).....	15
Figure 5: Prism layer mesh (CD-Adapco, 2011)	19
Figure 6: Extrusion mesh (CD-Adapco, 2011).....	20
Figure 7: Surface in 1D column of elements (left) and 2D grid (right) (Flow Science, n.d.).	21
Figure 8: Illustration of grids that are unsuitable (left) and suitable (right) for two-phase flows using the VOF model (CD-Adapco, 2011).	22
Figure 9: Grid generation principles.	28
Figure 10: Map overview, Surna.....	32
Figure 11: Aerial photo, Surna.....	32
Figure 12: Inflow hydrograph for the unsteady simulation.....	34
Figure 13: Bathymetry data points available for the digital elevation model of Surna (Pedersen, 2012a)	36
Figure 14: Digital elevation model, Surna, (riverbed elevation [masl]).....	36
Figure 15: Stage-Discharge curve for Surna (Pedersen, 2012a).	37
Figure 16: Roughness height calibration plot from preliminary project (Pedersen, 2012a).....	38
Figure 17: Cross section view of Star CCM+ grid (top) and SSIIM grid (bottom).	39
Figure 18: Map overview, Lundesokna (Coordinates are UTM 33N)	44
Figure 19: Aerial photo, Lundesokna.....	44
Figure 20: Lundesokna digital elevation model (z = riverbed elevation [m])	46
Figure 21: Water-line data plotted in ArcGIS.	47
Figure 22: Plot showing water lines. The data is split into an upstream and downstream section.	48
Figure 23: Plot of individual transects	49
Figure 24: Average transect and projected cross section plane.....	50
Figure 25: Snapshot from the video of the hydropeaking event.....	51
Figure 26: Sketch showing sediment sampling points, Lundesokna	52
Figure 27: Top-down plot of water-lines with varying roughness height close to the bend.....	54
Figure 28: Cross section view for Lundesokna grids. Top: m6 grid. Bottom: m7 grid	57
Figure 29: Mass balance plot for stationary simulation at 16.44 m^3 Results	59
Figure 30: Residual plot in Star CCM+	60

Figure 31: River bed elevation [m] (upper), and surface velocity vectors [m/s] (lower) for the Star CCM+ model, steady flow, Surna..... 61

Figure 32: Surface velocity magnitudes [m/s] from SSIIM, steady flow, Surna..... 62

Figure 33: Comparison of bed shear [Pa] in Star CCM+ (upper) and SSIIM (lower), steady flow, Surna. 63

Figure 34: Position of the cross-section for extracting velocities..... 64

Figure 35: Average velocities in a cross-section [m/s], steady flow, Surna..... 64

Figure 36: Bed shear force [Pa] , Left: SSIIM, Right: Star CCM+, unsteady flow, Surna 66

Figure 37: Left: Surface-velocity vector [m/s]. Right: Water depths [m], steady flow, Lundesokna 68

Figure 38: Top-down plot of simulated versus measured water-lines at 10.58 m³/s, steady flow, Lundesokna 69

Figure 39: Top-down plot of simulated versus measured water-lines at 16.44 m³/s, steady flow, Lundesokna 70

Figure 40: Top-down plot of simulated versus measured water-lines at 20.63 m³/s, steady flow, Lundesokna 70

Figure 41: Measured velocities (top left) and simulated velocities (top right) in a cross-section. Depth averaged velocity profiles [m/s] (bottom), steady flow, Lundesokna 72

Figure 42: Comparison of surface velocity vectors at 2 m³/s. Top: m6 grid. Bottom: m7 grid, steady flow, Lundesokna..... 73

Figure 43 Comparison of surface velocity vectors at 2 m³/s. Top: m6 grid. Bottom: m7 grid, steady flow, Lundesokna 74

Figure 44: Comparison of simulations with video footage, unsteady flow, Lundesokna 76

Figure 45: Surface velocity vectors [m/s], unsteady flow, Lundesokna 77

Figure 46: Spacing of geometry data in Surna. Top left: Spacing of cross sections, Top right: Spacing of echo sounder data, Bottom: Spacing in area close to island..... 80

Figure 47: Errors due to unphysical velocities..... 85

Figure 48: Velocity vectors and volume fraction of water in cross-sections. Top: Lundesokna, Bottom: Surna. 86

Tables

Table 1: Star CCM+ and SSIIM grid for the Surna site. 39

Table 2: Model setup for SSIIM and Star CCM+, Surna. 41

Table 3: Stage-discharge table for Lundesokna..... 48

Table 4: Overview over tested grids.....	53
Table 5: Grids used for modeling Lundesokna	56
Table 6: Model setup for Star CCM+, Lundesokna.	58
Table 7: Assessment of geometry data from Surna (Pedersen, 2012)	79
Table 8: Comparison of SSIM and Star CCM+ grid data.....	82

1 Introduction

1.1 Background

Over the next years it is expected that the hydropower peaking operations of Norwegian power plants will increase. Hydropower peaking is rapid changes in electricity production to meet peaks in demand and electricity prices. During peaking operation the power plant may rapidly increase or decrease the discharge through the plant, causing rapid changes in water-levels and velocity downstream. This may cause harm to fish, vegetation or invertebrates as well as cause changes in the fluvial geomorphology and water quality. In order to investigate the environmental effects of hydro-peaking, detailed knowledge of the hydraulic conditions in the river is important. 3D CFD modeling has recently become more popular for simulating the flow field in natural rivers. R  ther et al. (2010) and Spiller et al. (2011) provide a good overview of available research on the field.

This thesis seeks to investigate the capabilities of the 3D CFD codes SSIIM and Star CCM+ for modeling hydraulic conditions due to unsteady hydro-peaking effects.

Two rivers are modeled in this thesis, Surna in Surnadalen and Lundesokna by Lundamo. A map showing the location of the rivers in Norway can be found on the last page of this document (Appendix C).

Prior to this thesis the freeware CFD code SSIIM was used to model shear-forces at the river bed at steady flow conditions in the regulated river Surna (Pedersen, 2012a). The SSIIM model showed promising results, but good field data was not available for validation. The SSIIM model was further developed by the supervisor for this thesis, Associate professor Nils R  ther simultaneously with the thesis work. The project report from the earlier SSIIM modeling is available as a digital attachment (see Appendix A).

Several video files from unsteady simulations in Lundesokna are also available as digital attachments (Appendix A). These are part of the results from Lundesokna, and should be considered part of the thesis.

1.2 Focus and limitations

In Surna the focus of the study is to model the flow field and shear-forces at the bed for steady and unsteady flow. For steady flow the setup used in the preliminary project (Pedersen, 2012a) is used as a basis for modeling. A hypothetical hydro-peaking scenario is used as a basis for the unsteady simulation. Both steady and unsteady simulations in Star CCM+ are compared to the ones in SSIIM. In Lundesokna, the focus has been on modeling the flow field and water surface elevations in Star CCM+ for steady flow, as field data is available for validation of these variables. Video footage from a hydro-peaking event forms the basis for modeling unsteady flow. Only Star CCM+ was used for modeling Lundesokna.

Surface models were available in SSIIM from the preliminary project for Surna and from another project at EnviPEAK for Lundesokna. The modeling work done in this thesis is based on the available 3D surfaces and refines them into steady and unsteady flow models in Star CCM+. The focus has been on grid generation procedures, as this turned out to be a major factor in achieving good results.

For the physical setup the thesis is based on solving the RANS equations using a standard $k-\epsilon$ turbulence model for SSIIM and a realizable $k-\epsilon$ model for Star CCM+. Only one set up is used for each model, and experiments with different types of turbulence models or other physical or mathematical models such as discretization schemes and solvers are beyond the scope of this thesis and are not discussed here.

As the author had no prior experience with Star CCM+ before starting work on this thesis, part of the work has been to get familiarized with the software. In particular a lot of effort has gone into experimentation with grids for Surna. As details on these experiments are not interesting for this rest of the thesis work, no summary on this were written. Instead, the grid generation method outlined in chapter 5 shows the results of the experimentation.

1.3 Outline

Chapter 2 describes the most relevant basic theory on CFD. Chapter 3 describes the CFD packages SSIIM and Star CCM+, and explains how theory is implemented in the models. Chapter 4 is a very brief description of the hardware used. Grid experiments while modeling have led to the modeling method described in Chapter 5. Chapters 6 and 7 describe the two rivers, scenarios used, and the modeling process. The results from the simulations are presented in chapter 8, and discussed in chapter 9. The conclusion is found in chapter 10.

2 Numerical modeling of the Navier-Stokes equations

2.1 Introduction

The basis for the models is to obtain the velocity field by solving the Navier-Stokes equation numerically. The Navier-Stokes equations are derived by applying the basic principles of conservation of mass, momentum and energy on a small volume of water. For most cases the Navier-Stokes equations are nonlinear partial differential equations, making an analytical solution difficult or even impossible. Instead, the equations are often solved numerically for practical applications. The equations are then discretized and solved on each cell in a grid using the Finite Volume Method. This chapter aims to explain briefly how this is done.

2.2 Governing equations

For incompressible flow, the Navier-Stokes equations can be written as follows (Rodi, 1980):

$$\frac{\partial u_i}{\partial t} + u_j \frac{\partial u_i}{\partial x_j} = \frac{1}{\rho} \left(-\frac{\partial p}{\partial x_i} + \mu \frac{\partial^2 u_i}{\partial x_j^2} \right) + G$$

On the left side of the equation the two terms are a transient acceleration, and a convective acceleration respectively. The two first terms on the right is the pressure gradient and a viscose term. The term G represents the other body forces acting on the fluid, for example gravity and buoyancy forces.

The other equation needed to get a closed set of equations is the continuity equation. For an incompressible fluid (Rodi, 1980):

$$\frac{\partial u_i}{\partial x_i} = 0$$

It is common to use a Reynolds averaged version of the equations. Reynolds averaging is done by splitting the velocity variable into a time-averaged and a fluctuating part (Olsen, 2011b). This is illustrated in figure 1.

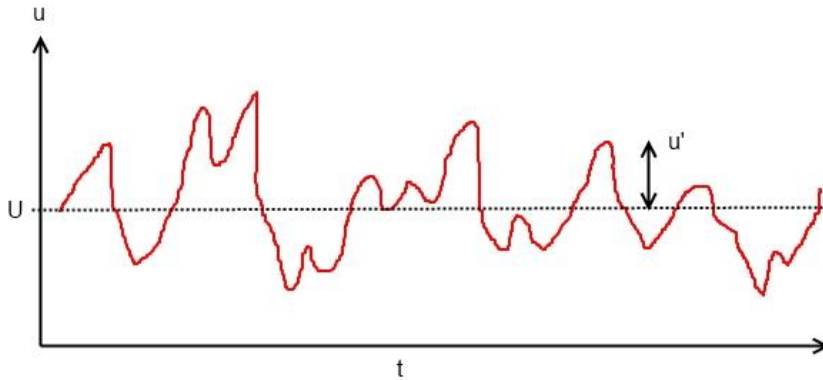


Figure 1: Reynolds averaging

Substituting $u = U + u'$ into the Navier-Stokes equation, taking the time-average and rearranging gives the Reynolds averaged Navier-Stokes equation (Weiming, Rodi, & Wenka, 2000):

$$\frac{\partial U_i}{\partial t} + \frac{\partial(U_i U_j)}{\partial x_j} = \frac{1}{\rho} \frac{\partial p}{\partial x_i} + \frac{1}{\rho} \frac{\partial \tau_{ij}}{\partial x_j} + G$$

The term τ_{ij} represents the time-averaged fluctuating velocities from the Reynolds averaging. The effect of the term can be seen as a diffusion of the momentum due to turbulence. As it works as an added stress on the fluid, it is often called the turbulent stress, or Reynolds stress. The correlation between the velocity fluctuation in i and j direction is unknown. Therefore the Reynolds stress is usually modeled by introducing another equation, the Boussinesq approximation (Weiming, Rodi, & Wenka, 2000):

$$\tau_{ij} = -\rho \nu_t \left(\frac{\partial U_i}{\partial x_j} + \frac{\partial U_j}{\partial x_i} \right) + \frac{2}{3} \delta_{ij} k$$

It is assumed here that the Reynolds stress is proportional to the mean velocity gradients. This introduces the eddy-viscosity ν_t , which then have to be modeled by a turbulence model.

2.3 Turbulence models

A central part of numerical modeling of flow is the use of turbulence models. One of the most used models is the k- ϵ model, and this model is used for all the modeling in this thesis. Therefore the focus in this chapter will be on the development and discussion of the k- ϵ model.

2.3.1 Modeling the eddy-viscosity

The basis for most RANS turbulence models is the modeling of the eddy-viscosity (ν_t) described in the previous chapter. The simplest way of modeling the eddy-viscosity is to set the value to a constant. This is mainly valid for large bodies of water, or “far-field” calculations, where the turbulent eddies are mainly created by the water body, and not disturbed significantly by the surrounding geometry. It has the most important application in depth-averaged calculations, where only the horizontal velocities are considered, and for calculating concentrations and temperatures when the velocity field is assumed to be known (calculated by more exact means). In cases of more complex flow conditions the turbulence will be affected by convective and diffusive transport, and generally transport equations can be employed to calculate the eddy-viscosity. Important here is the assumption that the eddy-viscosity is proportional to a velocity scale V' and a length scale L describing large scale turbulent eddies (Rodi, 1980):

$$\nu_t \propto V'L$$

Using a constant eddy-viscosity is a zero-equation model. One- and two- equation models indicate how many transport equations for the velocity and length scale are employed. An important one-equation model is the k model. The turbulent kinetic energy k can be calculated by the turbulent normal stresses (Rodi, 1980):

$$k = \frac{1}{2} \left(\overline{u_1'^2} + \overline{u_2'^2} + \overline{u_3'^2} \right)$$

Most of the kinetic energy is contained in the large scale turbulent motion. It therefore makes sense to use \sqrt{k} as a velocity scale for the large scale motion. This leads to the Kolmogorov-Prandtl equation for the eddy-viscosity (Rodi, 1980):

$$\nu_t = c'_\mu \sqrt{k} L$$

Here c'_μ is an empirical constant. In one-equation models a transport equation is employed for k , while L is often determined by simple empirical relations.

2.3.2 The k - ε model

For two-equation models the length scale is also modeled by a transport equation. The length scale is often expressed by the dissipation rate of the turbulent kinetic energy (Rodi, 1980):

$$\varepsilon \propto \frac{k^{3/2}}{L}$$

This gives the scaling of ν_t for the k - ε model:

$$\nu_t = c_\mu \frac{k^2}{\varepsilon}$$

The k - ε model employs transport equations both for k and ε . The transport equations can be written as follows (Weiming, Rodi, & Wenka, 2000):

$$\begin{aligned} \frac{\partial k}{\partial t} + U_i \frac{\partial k}{\partial x_i} &= \frac{\partial}{\partial x_i} \left(\frac{\nu_t}{\sigma_k} \frac{\partial k}{\partial x_i} \right) + P - \varepsilon \\ \frac{\partial \varepsilon}{\partial t} + U_i \frac{\partial \varepsilon}{\partial x_i} &= \frac{\partial}{\partial x_i} \left(\frac{\nu_t}{\sigma_\varepsilon} \frac{\partial \varepsilon}{\partial x_i} \right) + c_{1\varepsilon} \frac{\varepsilon}{k} P - c_{2\varepsilon} \frac{\varepsilon^2}{k} \\ P &= \nu_t \left(\frac{\partial U_i}{\partial x_j} + \frac{\partial U_j}{\partial x_i} \right) \frac{\partial U_i}{\partial x_j} \end{aligned}$$

Here the term P is the production of turbulent kinetic energy. σ_k , σ_ε , $c_{1\varepsilon}$, $c_{2\varepsilon}$ and c_μ are empirical constants that can be determined experimentally. In the k - ε model these constants are:

$$\sigma_k = 1.0 \quad \sigma_\varepsilon = 1.3 \quad c_{1\varepsilon} = 1.44 \quad c_{2\varepsilon} = 1.92 \quad c_\mu = 0.09$$

The model described above is often called the *standard* k- ϵ model. A more recent successful development is the *realizable* k- ϵ model. This model was developed by Shih et al. (1994), and provides better results than the standard k- ϵ model for many applications. It involves a new transport equation for ϵ , and the c_μ parameter is expressed as a function of the mean flow and turbulence properties, rather than being expressed as a constant (CD-Adapco, 2011).

2.4 Grids

In order to transform the Navier-Stokes equations on differential form into a solvable form, the solution domain should be transformed into a set of finite cells called a grid or a mesh. (In this thesis both terms will be used interchangeably). The idea is to discretize the Navier-Stokes equations and then solve the equations at discrete points, either inside the cells, or at the intersections between them. For a 2D-grid the cells are normally triangular or quadrilateral and for a 3D-grid usually tetrahedral, hexahedral, prismatic or pyramidal (Blazec, 2005).

In general there are two types of grids, *structured grids* and *unstructured grids*. Only unstructured grids are covered here, as the CFD codes used in this thesis uses this type of grid. Unstructured grids are grids that cannot be identified by an index, i.e. the number of rows or columns of cells in a 2D grid changes through the model.

The main advantage of unstructured grids is that it is much easier to fit the grid to a complex geometry, the disadvantage is that more complex code must be added to the solver in order to identify neighboring cells. However, as most engineering problems involve complex geometries, the advantage of the flexibility greatly outweighs the problem of solver complexity for many problems. Most commercial CFD-codes today therefore use unstructured grids (Blazec, 2005). It is common to use an unstructured grid with a mix of different cells, for example hexahedral, polyhedral and prismatic cells. Figure 2 shows a 3D grid with hexahedral and polyhedral cells on the left, and the same grid using tetrahedral cells on the right:

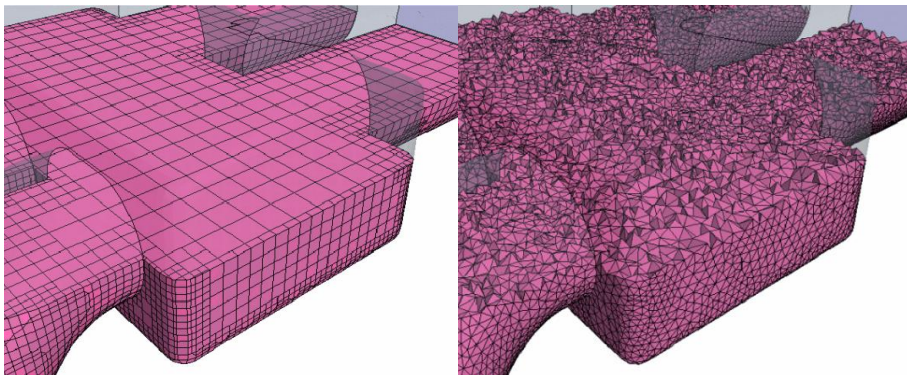


Figure 2: unstructured 3D grids from Star CCM+ (CD-Adapco, 2011). Left: Mix of hexahedral and polyhedral cells. Right: tetrahedral cells.

2.4.1 Grid quality

The way the grid is constructed may be important both for the accuracy and convergence of the solution, especially when modeling complex geometries. In order to increase the accuracy of the solution at the wall boundaries, it is recommended to place a “prism-layer” close to the boundary (Blazec, 2005). This is one or more layers of prismatic cells that are orthogonal to the wall boundary surface. The shape of the cells in the grid is also important. Olsen (2011b) lists three cell characteristics that are important:

- Non-orthogonality: This means the magnitude of the angle of the grid line intersection. This should be as close to orthogonal as possible
- Aspect ratio: The ratio between the cells lengths in x, y and z direction. The anisotropy of cells should not be too large.
- Expansion ratio: The size difference between neighboring cells. The expansion ratio should not be too large.

2.5 Discretization of the convective and diffusive terms

Several methods exist for discretizing the equations, notably the finite difference method, the finite volume method and the finite element method. Because of its flexibility and ease of implementation the finite volume method is particularly well suited for the treatment of flow in complex geometries (Blazec, 2005). This is also the method used in most 3D codes, including Star CCM+ and SSIIM. The main idea of the finite volume method is the division of the solution domain into a number of control-volumes. For these control-volumes conservation can be stated by setting the sum of fluxes over the control-volume surface equal to zero or to a source term. Murthy (2002) illustrates this with the example of one dimensional diffusive flux with a source term:

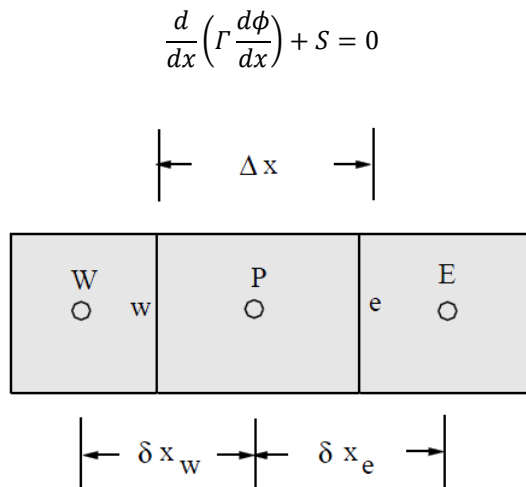


Figure 3: Arrangement of Control Volumes (Murthy, 2002)

Consider the control volumes in figure 3, here W and E are calculation nodes at the western and eastern cell and w and e denote the walls of cell P. The next step is to integrate the equation over cell P (Murthy, 2002):

$$\int_w^e \frac{d}{dx} \left(\Gamma \frac{d\phi}{dx} \right) + S dx = 0 \Rightarrow$$

$$\left(\Gamma \frac{d\phi}{dx} \right)_e - \left(\Gamma \frac{d\phi}{dx} \right)_w + \int_w^e S dx = 0$$

Then the equation is discretized. To do that, we make an assumption of how ϕ varies. If the assumption is that ϕ varies linearly between the nodes the equation becomes (Murthy, 2002):

$$\frac{\Gamma(\phi_E - \phi_P)}{\delta x_E} - \frac{\Gamma(\phi_P - \phi_W)}{\delta x_W} + \bar{S}\Delta x = 0$$

Similar discretization can be done for a 2D or 3D situation and for more complex cells.

2.5.1 Upwind differencing

For convective terms it makes more sense to calculate the quantity in cell P (Figure 3) only from cells upstream of this cell. This is because the convective transport of the quantity in question only is transported in the flow direction, while the diffusive transport is dependent of the gradient of the quantity. This is called *upwind* differencing.

Upwind schemes are usually called first-order schemes (FOU) if only one upstream cell is used and second-order schemes (SOU) if two cells are used.

A problem with first order schemes is that they are very diffusive (Murthy, 2002). If the flow direction is not aligned with the grid, the approximation error made in the discretization of the equation will cause the quantity to diffuse to neighboring cells. The severity of this error depends on the coarseness of the grid and the discretization scheme used. Because the error gives an apparent diffusion, it is often called false diffusion.

A commonly used first-order scheme is the Power-law Scheme. In this scheme the diffusive flux is multiplied with a reduction factor (Olsen, 2011b):

$$f_p = (1 - 0.1|Pe|)^5$$

Where Pe is the Peclet number:

$$Pe = \frac{U\Delta x}{\Gamma}$$

This means that the reduction of the diffusion is dependent on the ratio of the convective to the diffusive flux. The reduction factor decreases with the relative size of the convective flux, and helps to reduce the effects of false diffusion.

Using second order schemes will generally make the solution converge more slowly, but will reduce the effects of false diffusion, as shown in R uther et al. (2010).

2.6 Boundary conditions

Boundaries are the surfaces that surround the solution domain. Setting some boundary conditions is necessary to get a closed set of equations that can be solved from the discretized Navier-Stokes equations. The types of boundaries usually used for a free-surface calculation is:

- Inflow boundaries
- Outflow boundaries
- Wall boundaries

In addition, for calculations of symmetrical flows it is only necessary to calculate half the flow region, and then a symmetrical boundary can be specified to save computational power (Rodi, 1980).

2.6.1 Wall laws

Wall laws are functions that define how the transition between the laminar flow close to a wall boundary and turbulent regions further out from the wall are handled. It is generally assumed that the turbulence model used is only valid outside of the viscous-dominated sub region with laminar flow. In a wall-function approach the velocities are described as a linear function in the viscous-dominated region close to the wall, and a logarithmic function further out. Some wall laws also model a buffer region to smooth out the transition between the laminar and logarithmic region.

The equivalent sand-grain roughness height (k_s , hereafter referred to as the “roughness height”) is a parameter first established by Nikuradse (Labioud, Godillot, & Caussade, 2007). It is a theoretical size corresponding to the diameter of equally sized sand spheres on a surface. This is illustrated in figure 4. The roughness height is used as an input parameter in the wall law formulations both in Star CCM+ and SSIIM.

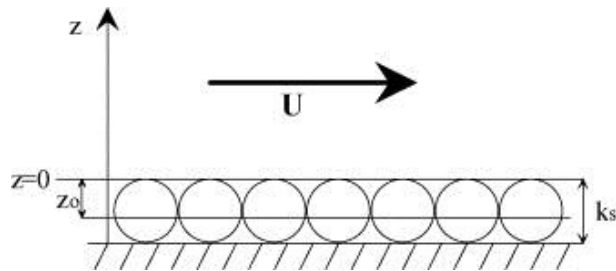


Figure 4: Equivalent sand-grain roughness height (k_s) (Labioud, Godillot, & Caussade, 2007)

Because of the way the wall laws are formulated, the roughness height should be smaller than the distance to cell centroid of wall adjacent cells to avoid unphysical results (CD-Adapco, 2011). In Star CCM+ this will automatically be enforced, while SSIIM will allow larger roughness heights.

3 Software

3.1 Star CCM+

3.1.1 Introduction

Star CCM+ is a commercial CFD package that includes a 3D-CAD modeler, meshing tools, multiple CFD models and solvers, and post-processing tools. The program is designed to solve a wide range of CFD problems, ranging from aerodynamics to mixed flow problems in pipes, and free surface flows and waves (CD-Adapco, 2011).

3.1.2 Physics models

Star CCM+ includes both implicit and explicit unsteady models. For modeling turbulence it includes several RANS models, including the standard and realizable k- ϵ models, as well as Reynold's Stress (RSM) and LES / DES capabilities. Fluids can be modeled as ideal gas, real gas, or incompressible. Multiphase model capabilities include VOF and Eulerian multiphase (CD-Adapco, 2011). For modeling free surface flows a multiphase-model can be combined with VOF algorithms.

3.1.3 Boundaries

Star CCM+ incorporates several types of boundaries including (CD-Adapco, 2011):

- *Velocity inlet*: Inflow is defined as a velocity vector field.
- *Mass-flow inlet*: The inflow is defined as mass per unit time.
- *Stagnation inlet*: Inflow is defined by a known stagnation pressure.
- *Split flow outlet*: The fraction of fluid exiting through the outlet is defined.
- *Pressure outlet*: The static pressure is defined at the boundary.

The split flow outlet uses zero-gradient conditions, but is not suitable for outlets where reverse flow (inflow) occurs (CD-Adapco, 2011). For the pressure outlet boundary a special algorithm is used to reduce the problem with reverse flow (CD-Adapco, 2011). The formula reduces the pressure where inflow occurs at the outlet by the dynamic head:

$$p = p_{\text{specified}} - \frac{1}{2} \rho |u_n|^2$$

Here $p_{\text{specified}}$ is the pressure specified at the boundary while u_n is the normal component of the boundary inflow velocity

3.1.3.1 *Wall laws*

Star CCM+ employs three different models for near-wall treatment, the high-, low- and all- y^+ models (CD-Adapco, 2011). The high- y^+ model assumes that the cell closest to the wall is within the logarithmic region of the boundary layer, while the low- y^+ model assumes that the grid is so fine that the viscous sub-layer is properly resolved. The all- y^+ model is a hybrid that uses low y^+ for fine meshes and high y^+ for coarser meshes. It is also formulated to produce more reasonable results for intermediate meshes.

3.1.4 *Mesh generation*

For making a mesh, Star CCM+ includes a Volume mesh generator as well as surface treatment tools. In order to make a grid, a 3D surface file can be imported. This can for instance be a CAD file representing the geometry that is to be modeled. The surface mesher then uses the imported surface to make a refined surface mesh, and then this mesh is the starting point for generating the volume mesh. The different core meshers available are (CD-Adapco, 2011):

- Tetrahedral
- Polyhedral
- Trimmed
- Thin mesh

The tetrahedral and polyhedral meshers generate meshes based on tetrahedral, and polyhedral cell shapes, the thin mesher does the same, but has special algorithms for generating meshes in very thin areas. The trimmer mesher makes a mesh of mainly hexahedral cells that can be aligned in the direction of a coordinate system of choice. The trimmer mesh will make automatic refinements close to wall boundaries when needed. Volume shapes like boxes, spheres or cylinders can also be added in the model to refine cells in areas of interest. When using hexahedral cells it is also possible to use volume shapes to define anisotropic cell dimensions. In addition it is possible to change cell sizes at the boundaries. In order to control the expansion ratio of cells between refined areas and the core mesh, a growth rate can be used. The growth rate defines how many cells shall be used to make a smooth transition between the refinement and core mesh.

In addition to the core meshers, Star CCM+ has the option of adding a prismatic near wall mesh (CD-Adapco, 2011). This mesher makes one or more layers of fine orthogonal prismatic cells next to the wall boundaries in order to improve the accuracy of the solution. The prism layer can be defined by its normal thickness from

the wall, and by a stretching parameter that defines the expansion ratio between neighboring layers. Figure 5 illustrates a prism layer mesh with two layers.

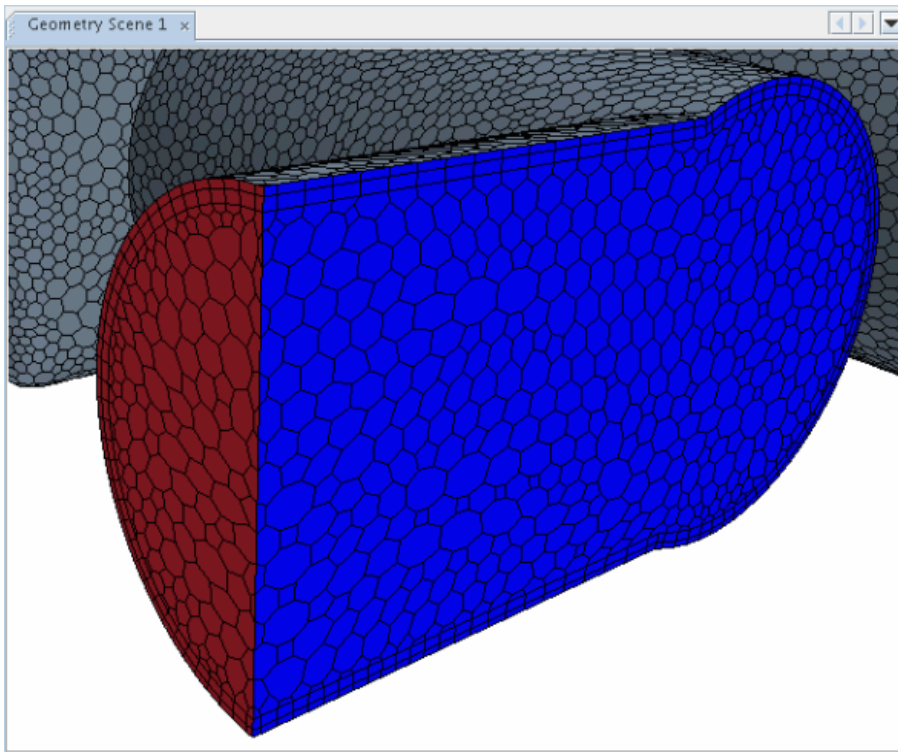


Figure 5: Prism layer mesh (CD-Adapco, 2011)

It is also possible to add orthogonal cells at boundaries using the extrusion mesher. This is useful to extend the conditions at inlet or outlet boundaries so that the model gives a better representation of the prototype conditions. Figure 6 shows an extrusion mesh (and also includes a prism layer).

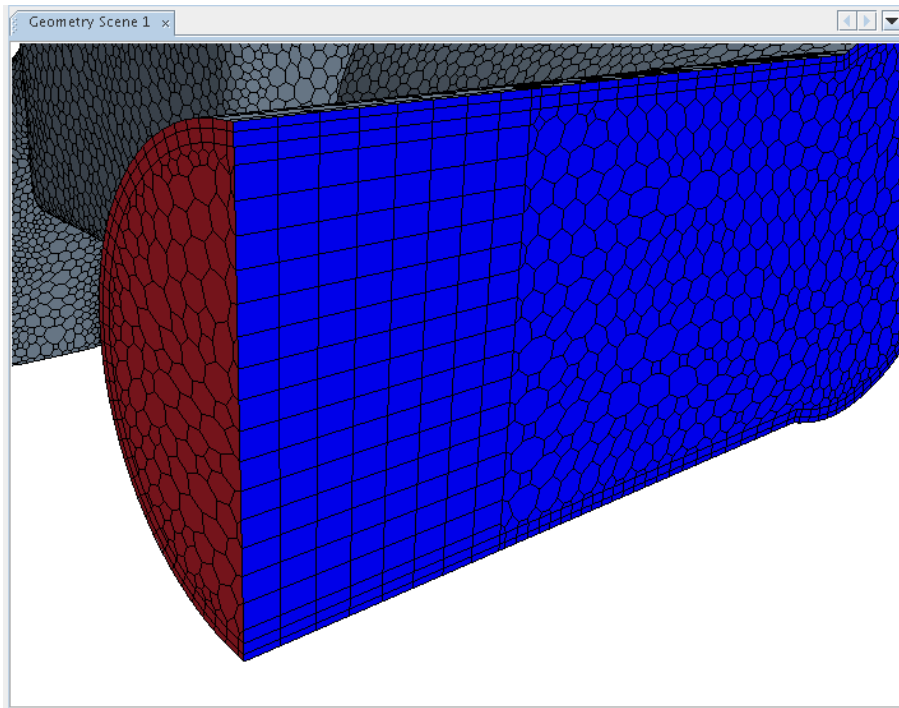


Figure 6: Extrusion mesh (CD-Adapco, 2011)

In Star CCM+ the grid can also be refined locally by using the tool “Volume shapes”. A volume can then be defined where special mesh and physics parameters can be set. This also makes it possible to make anisotropic cells.

3.1.5 Volume of fluid (VOF) algorithms

In Star CCM+ it is possible to use a two-phase Volume of Fluid method to calculate the location of the water surface. The method was first proposed by Hirt and Nichols (1981). As proposed here it is a method to resolve free-boundaries. A free-boundary can be an interface between fluids, like for free-surface flow, or it can be the interface between materials, or between a fluid and a deformable structure. In Star CCM+ the VOF method is used to resolve the boundary between two phases of fluid.

The basis of the VOF method as presented in Hirt and Nichols (1981) is that for each cell in the grid a water fraction function F is defined so that F is 1 if the cell is filled with fluid and 0 otherwise. A cell partly filled with fluid has a water fraction between 1 and 0. It is thus clear that cells with a fraction other than 1 or 0 must contain a free water surface. The exact position of the surface can then be calculated. As illustrated in figure 7 this is straight forward for a one-dimensional column. The location of the water surface location simply becomes the level of the bottom of the cell + F times the vertical size of the cell (Flow Science, n.d.). For two- and three-dimensional cases the calculation is a bit more involved because the slope of the water in a cell is not given, however the basic principle is the same.

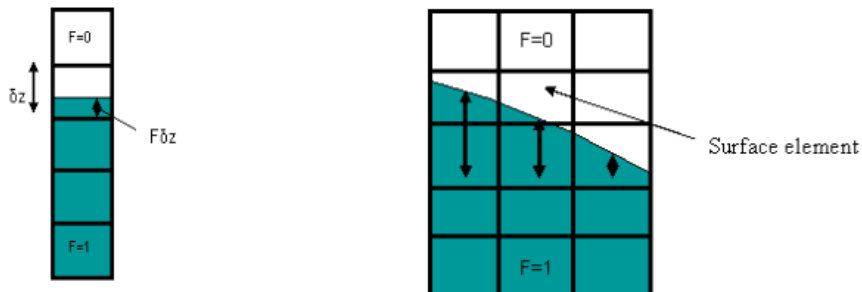


Figure 7: Surface in 1D column of elements (left) and 2D grid (right) (Flow Science, n.d.).

For a transient simulation the fluid fraction of each cell can be calculated by the following equation in 2D (Hirt & Nichols, 1981):

$$\frac{\partial F}{\partial t} + u_1 \frac{\partial F}{\partial x_1} + u_2 \frac{\partial F}{\partial x_2} = 0$$

In the Star CCM+ user guide (CD-Adapco, 2011) the VOF model is described as suitable for “simulations of flows where each phase constitutes a large structure, with a relatively small total contact area between phases”. Figure 8 illustrates this.

An assumption for the VOF method is that both phases share the same velocities, pressure and temperature within a control-volume (Hirt & Nichols, 1981). This assumption will lead to large errors if the fluid bodies are small compared to the fineness of the grid. At least three cells should be used across the water body to get good results (CD-Adapco, 2011).

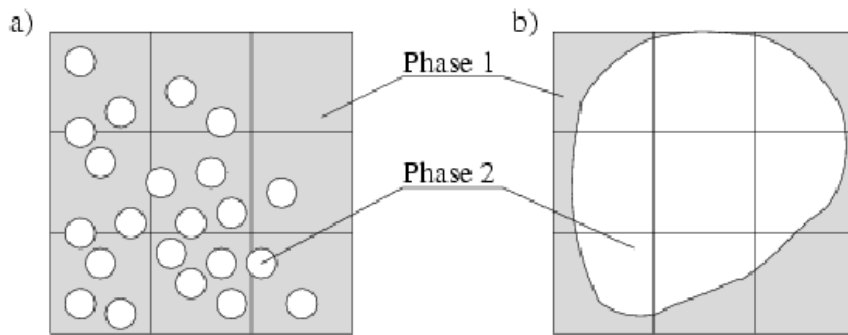


Figure 8: Illustration of grids that are unsuitable (left) and suitable (right) for two-phase flows using the VOF model (CD-Adapco, 2011).

3.2 SSIIM

3.2.1 Introduction

The numerical model SSIIM is an in-house CFD code developed by Olsen (2011a), (2011b) at the Norwegian University of Science and Technology. SSIIM was primarily designed to solve sediment-transport problems in intakes, but have later been further developed to solve various other sediment and flow problems. SSIIM comes in two versions, SSIIM 1 which uses a structure-grid, and SSIIM 2 which uses an unstructured-grid with the possibility of using an adaptive grid that follows the water surface. This is further explained below. The version used in this thesis is SSIIM 2, and it is simply referred to as SSIIM in the further.

3.2.2 Physics models

SSIIM solves the 3D RANS equations using the standard k-epsilon turbulence model as described by Rodi (1980) by default. In addition it is possible to use more simple turbulence models (zero-equation models, and constant Eddy-viscosity), as well as the Spallart-Allmaras one-equation model, and the k- ω two-equation model. The semi-implicit method for pressure linked equations (SIMPLE) is used for solving the pressure term (Patankar, 1980). The Power-Law Scheme or the second order upwind scheme can be used for discretization of the convective terms.

SSIIM uses a quasi-unsteady approach for modeling transient conditions. This means that continuity has to be satisfied for the model globally at any time-step, i.e. the discharge at inlets must equal the discharge at outlet. Consequently SSIIM is able to model a global transient water surface elevation rise, but is unable to model the effects of a wave traveling through the model.

The default wall law used in SSIIM is an empirical formula for the velocity profile given in Sclichting (1979):

$$u = \frac{1}{\kappa} \ln \left(\frac{30y}{k_s} \right) u^*$$

3.2.3 Adaptive grid approach

In SSIIM the water surface location for transient flow conditions can be computed by using the calculated pressure field. The water surface location is then calculated using the Bernoulli equation as follows (Haun & Olsen, 2012):

$$\frac{\partial p}{\partial x_i} = \rho g \frac{\partial z_s}{\partial x_i}$$

A reference cell with known water surface position is given as an input parameter. The pressure difference between the reference cell and any other surface cell is then related by the elevation difference between the two cells. This calculation is done for each time step, and the grid is updated to follow the water surface location. The method is further described in Olsen & Haun (2010). A grid that follows the water surface like this is often called an adaptive grid.

4 Hardware

Since the simulations are demanding in computer power, the hardware available becomes important. Three systems have been used for running simulations in this thesis:

- An Intel Core 2 Duo 3 GHz CPU with 4 GB of RAM owned by author
- Two Intel Core i7 3/3.4 GHz CPUs (4 cores) with 16 GB of RAM supplied by the department of Hydraulic and Environmental engineering.

For the m6 grid used for most of the computations in Lundesokna, the two last computers use approximately 3-4 seconds per iteration. At 0.1 second time steps and 4 inner iterations per time step this makes for about 120 seconds computational time per second physical time. For the steady simulations equilibrium is reached after about 12 minutes. The computational time for a steady simulation is then about 24 hours. Another 24 hours is used to calculate the development in the unsteady flow calculation. The unsteady flow simulation in Lundesokna, using the much finer m7 grid, was calculated in approximately 7 days.

5 Grid generation method

This chapter describes the grid generation method used for making the final grids in Star CCM+. Over 20 different grids were tested during the modeling process for Surna. The method presented here is the result of the grid tests combined with theoretical considerations described in section 2.4 and 3.1.4. It is also inspired by the work done by Spiller et al. (2011) for generating a grid for Nidelva.

Star CCM+ has several possibilities for which cell types to use for modeling (section 3.1.4). Experiments were done with both the polyhedral and the trimmer mesher. Using polyhedral cells can sometimes give the same accuracy with fewer cells compared to using hexahedral cells because more neighboring cells can be used for the calculation. It was still decided to go with hexahedral cells (using the trimmer mesher), mainly because:

- The non-uniform positioning of polyhedral cells in the vertical direction causes an uneven water surface to be calculated when using VOF. This effect is bigger when few cells in the vertical direction are used.
- More importantly the possibilities when using refinements with trimmer cells are greater. In particular it is possible to use anisotropic cells and refined areas can be more sharply defined, since the trimmer cells have straight-line intersections between cells. This causes equivalent refinement to be possible with fewer cells.

Free surface flows are modeled by a two phase model with water and air phases in Star CCM+ (section 3.1.2). The VOF method is then used to calculate the interface between the phases. However, only the water phase is of interest for most free surface flow simulations. Consequently, computational time spent on cells containing only air should be as limited as possible. Reduced computational time can be achieved by using large cells in areas of the computational domain where the water fraction is 0 at all times (the “passive area”). A refinement can then be added in areas where the water fraction > 0 at some point during computations (the “active area”) by using the Volume shapes tool.

Figure 9 shows a grid section from the grid used in Lundesokna (m6) showing the course grid in the passive area and the refinement in active areas.

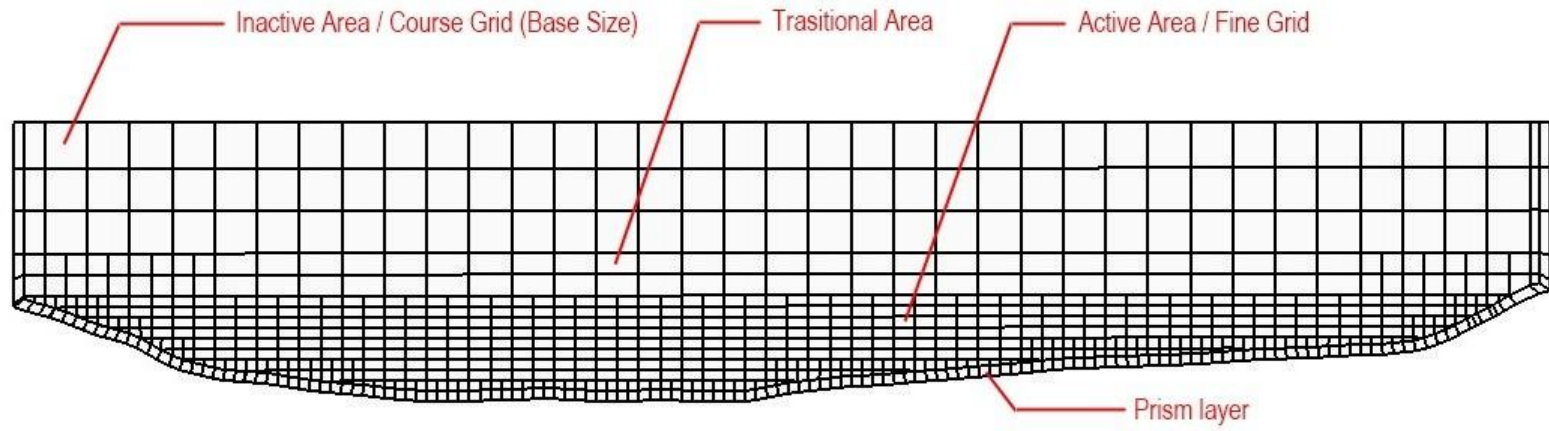


Figure 9: Grid generation principles.

Because the expansion rate should not be too large (section 2.4.1), a transitional area is defined. This can be controlled by setting the “default growth rate” condition in star CCM+. In the transitional area the cell sizes are gradually changing between the active area refinement and the passive area coarse grid.

The active area refinement also employs anisotropic cells with smaller cell sizes in the vertical direction. The VOF method generally requires 2-3 cells or more over the water depth to properly resolve the water surface (section 3.1.5). Because of this, finer cells are needed in the vertical direction to capture the water surface at low flows.

A prism layer is employed close to the bed to obtain better accuracy (see section 3.1.4). A problem that was encountered for both the rivers is that while fine cells are required close to the bed the wall laws formulation require that the roughness height parameter should be smaller than half the vertical cell size (section 3.1.4). This is further discussed in section 9.3. As a compromise the prism layers size is set equal to the active area refinement.

6 Modeling Surna

6.1 Background

The preliminary project preceding this master thesis involved investigating the capabilities of SSIIM to model bed shear forces during steady flow conditions in the river Surna (Pedersen, 2012a). The model produced reasonable flow fields and shear forces at the bed. There was, however, a lack of field data available for validation of the results. Therefore, it was decided to build a Star CCM+ model for steady flow and compare the results. The focus in this thesis is modeling hydraulic conditions due to hydro-peaking effects. In this respect unsteady conditions are of particular interest. The SSIIM model as well as the Star CCM+ model was therefore further developed to run unsteady flow simulations. The further development of SSIIM was conducted by Associate Professor Nils R  ther, who also is the supervisor for this project. The modeling in Star CCM+ is treated in this chapter.

The data basis for the DEM, as well as sediment data and hydrological data were gathered during the preliminary project, and is used for both the SSIIM and Star CCM+ model. The data is described briefly in this chapter. More detailed information both on collecting field data and data treatment can be found in the project (Pedersen, 2012a).

Successfully generating a grid for the Star CCM+ model in Surna proved difficult. Over 20 different grids were tested. In the end a grid was used that provided comparable results to the SSIIM model (see section 8.1.1), but the grid still has problems. Detailed information about the grid experiments is not considered interesting for this thesis and will not be treated here. The experience from this process is instead provided in the grid generation method described in chapter 5.

6.2 Site description

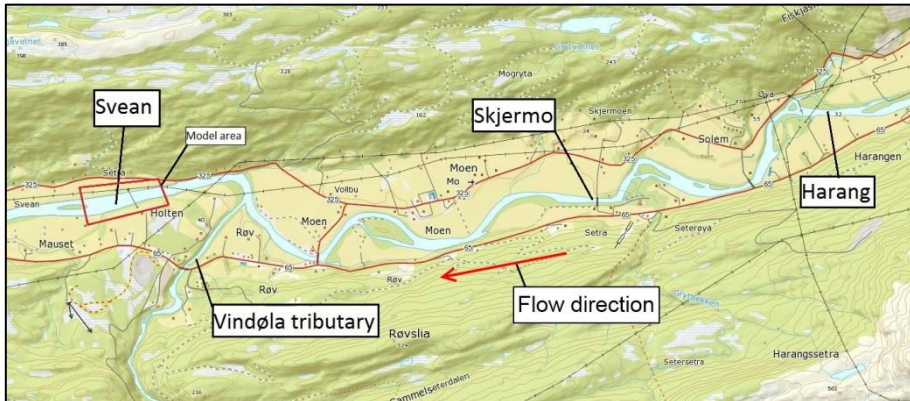


Figure 10: Map overview, Surna



Figure 11: Aerial photo, Surna

The study area is a straight river reach near Svean in the river Surna, located about 100 km south-west of Trondheim in Surnadalen in More and Romsdal (figure 11). The field site lays some 5 km downstream of the outlet of the Trollheim power plant and the Skjerme discharge measurement station. The modeled reach is about 480 meters long and broadens from approximately 80 meters upstream to 140 meters downstream.

A map showing the location of the Surna and Lundesokna in Norway can be found on the last page of this thesis (Appendix C).

The reach is characterized by an island just downstream of the modeled stretch where the main stream is separated. In the area just upstream of the island the river is shallow with depths as low as 30 cm during average discharge conditions. On the left side further upstream there is a deep scour hole. At normal flow the water depth in the hole is about 2 meters. The right bank is shallow all the way through the model. The river bed sediment consists mostly of gravel and cobbles, with an average particle size of approximately 7 cm.

6.3 Hydro-peaking scenario

Surna is currently not operated as a hydro peaking system. Therefore part of the assignment in this thesis was to come up with a hydro-peaking scenario. The focus of the thesis however is to model hydro-peaking effects in general, not to make a realistic scenario for Surna in particular. Therefore it was considered sufficient to come up with a plausible hydro-peaking scenario without regard to the realism of this scenario in Surna.

As a basis for the Hydro-peaking scenario, it was decided to look at Nidelva because:

- It is a Norwegian regulated river, comparable to Surna.
- Hydropeaking data exist for the river.

Nidelva is run as a hydropower scheme with discharges varying between 30 – 110 m³/s (Halleaker, et al., 1999). According to Halleaker et al. (2007) the minimum environmental flow from the Trollheim power plant is 15 m³/s. As Vindøla with a mean annual discharge of 5.8 m³/s runs into Surna between Trollheim and the study site, it was decided to use 20 m³/s as a minimum discharge. The maximum operating flow at Trollheim is 38.5 m³/s. As it was desirable to test a larger range than 20 -40 m³/s, it was decided that a scenario with twice the discharge should be used, making the maximum 80 m³/s. Finally it was decided that the scenario should be run with 20 minutes watering, 20 minutes steady flow to stabilize and 20 minutes dewatering. A hydrograph was created based on these values. The hydrograph is presented in figure 12.

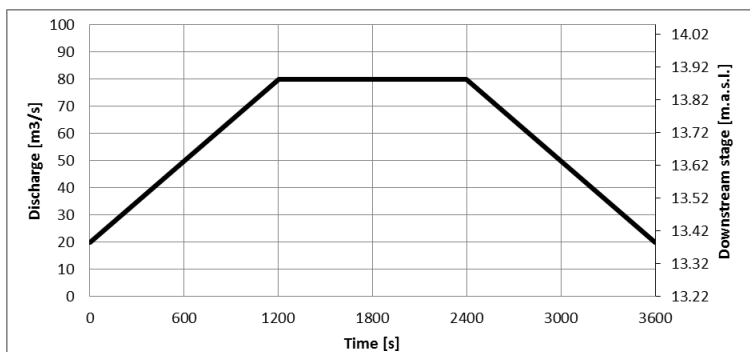


Figure 12: Inflow hydrograph for the unsteady simulation

6.4 Data basis

Part of the data basis for Surna was collected during the preliminary project (Pedersen, 2012a). The rest was available through EnviPEAK.

6.4.1 *Bathymetry and digital elevation model*

During the preliminary project (Pedersen, 2012a) bathymetry data were collected and a digital elevation model was prepared for use in SSIIM.

The bathymetry data needed for the model were gathered by Differential GPS or total station surveys. Data were collected in several ways:

- Data were collected in cross-sections by GPS-rover in areas shallow enough.
- Data were collected by echo-sounder in areas too deep for wading.
- In the area just upstream of the island data were collected in a fine grid, also by GPS-Rover.

The surveys were conducted using differential GPS.

In addition to the bathymetry data, points were extracted from digital elevation curves with 1 meter equidistance for points outside the river channel.

Figure 13 shows a plot of available geometry data in ArcGIS. The data was transformed to a surface model by using interpolation routines available in SSIIM. The data was then exported as a .stl 3D surface file that can be imported directly in Star CCM+. The final DEM in Star CCM+ is shown in figure 14.

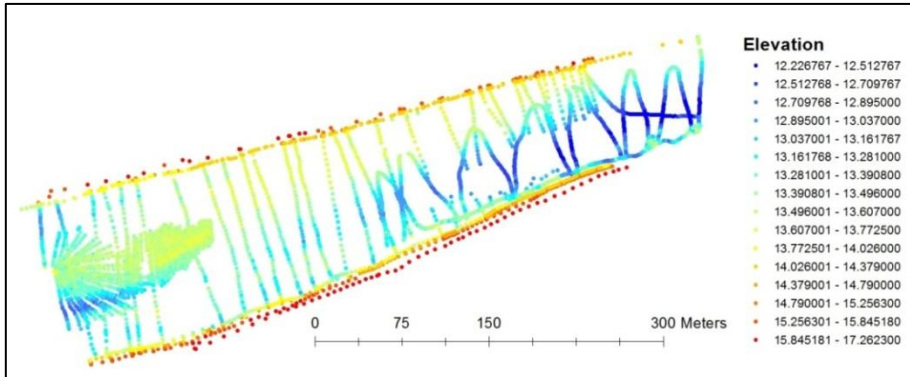


Figure 13: Bathymetry data points available for the digital elevation model of Surna (Pedersen, 2012a)

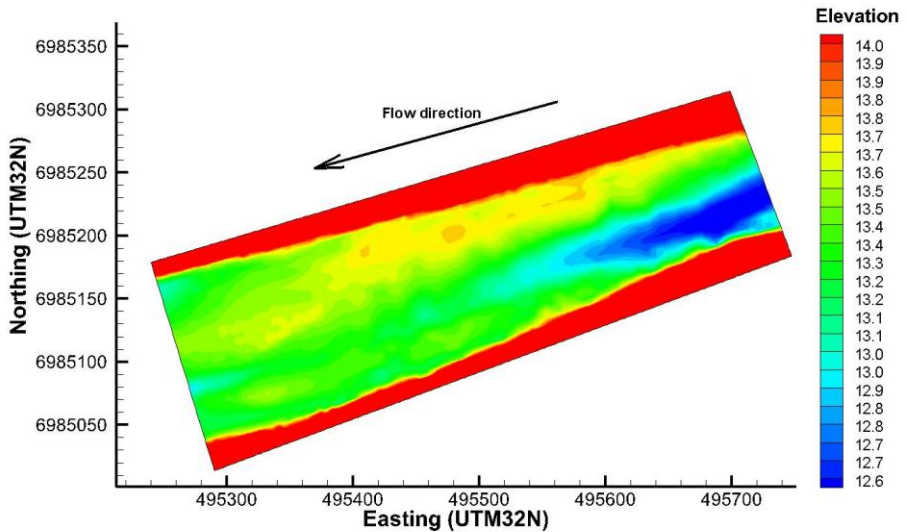


Figure 14: Digital elevation model, Surna, (riverbed elevation [masl])

6.4.2 Hydrology

Water surface elevation measurements were available for 60.37 m³/s and 48.46 m³/s discharges. The measurements were used both for calibrating a stage-discharge curve, and for calibrating the roughness height values for the model during the preliminary project (Pedersen, 2012a).

A stage-discharge curve was prepared during the preliminary project to estimate the upstream and downstream stages in the model for various discharges (Pedersen, 2012a). The curve was made by relating discharge data from Skjermo gauging station to pressure logger data from the study area. The stage discharge curve is shown in figure 15.

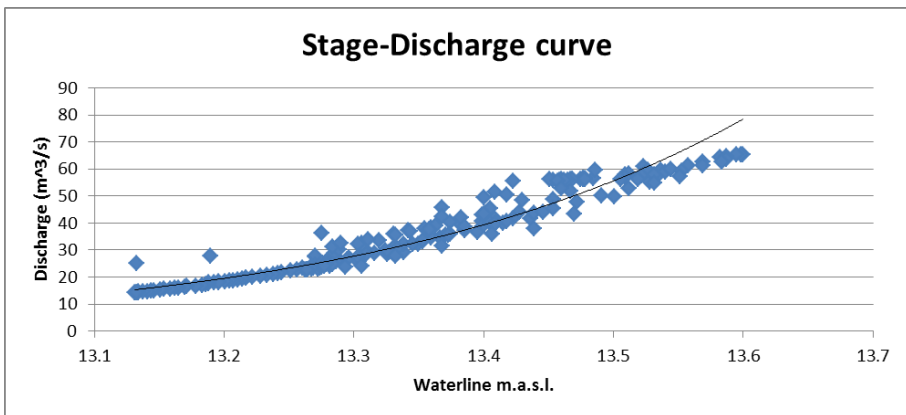


Figure 15: Stage-Discharge curve for Surna (Pedersen, 2012a).

Velocity measurements by ADCP were available for the 48.48 m³/s discharge. These data were of very poor quality and have not been used in this project.

6.4.3 Sediment data

Particle size distributions were obtained during the preliminary project by sieving analysis of bed surface probes. The data were used for obtaining estimates of the roughness height. Using Van Rijn's (1984) empirical formula, an estimate of the roughness height was 0.33 meters. The final roughness height used was obtained by calibration, and the estimates were then compared to the calibrated value.

6.5 Calibration of the roughness height

During the preliminary project the roughness height parameter was calibrated to be used as an input-parameter in the SSIIM. The result from the calibration was that a roughness height of 0.28 m gave the best fit (Pedersen, 2012a). Figure 16 shows polynomial regression lines of the simulated and measured water surface elevations. The roughness height of 0.28 meters was also used for simulations in Star CCM+.

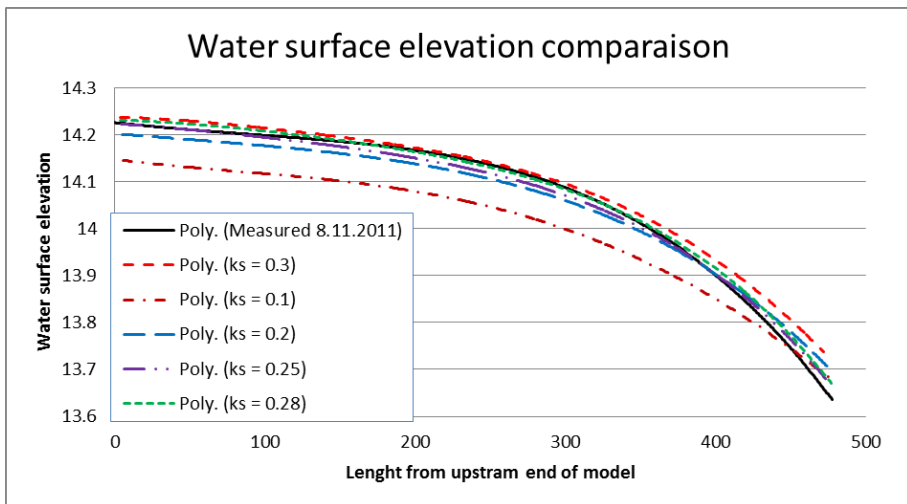


Figure 16: Roughness height calibration plot from preliminary project (Pedersen, 2012a).

6.6 Grids

Table 1 sums up the grid properties for both the Star-CCM+ model and the SSIIM model used. The SSIIM model uses an adaptive grid, which means that only cells in the water phase have to be modeled. This explains the lower cell count as well as the finer grid. A discussion on the two grids can be found in section 9.2.1. Figure 17 shows a cross-section view of the final Star-CCM+ grid together with the adaptive SSIIM grid. (Note that the grids are not in the same scale). In the SSIIM grid, the water-surface is the blue line. In the Star CCM+ grid, the water surface will be somewhere in the active area.

	Star CCM+	SSIIM
Cell count:	605,769	450,000
Cell type:	Trimmer mesh	Trimmer mesh
Passive area cell size	2.8 meters	Not available
Active area refinement cell size	Horizontal: 1.4 meters Vertical: 0.7 meters	Horizontal: 1 meter Vertical: 0.2 meters
Prism layer	Approximately 0.7 meters, two prism layers.	Not available

Table 1: Star CCM+ and SSIIM grid for the Surna site.

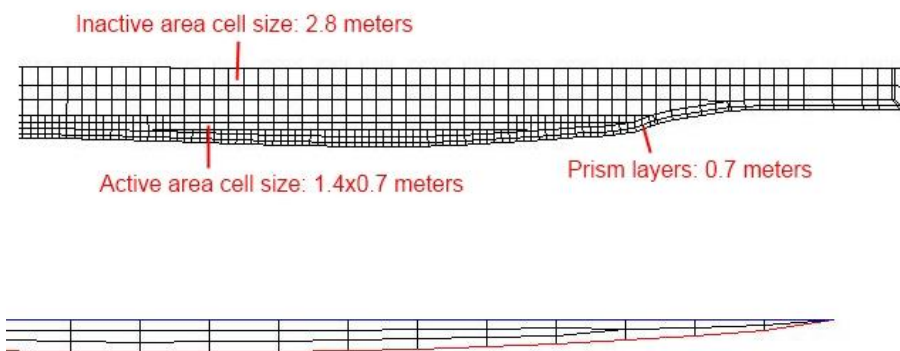


Figure 17: Cross section view of Star CCM+ grid (top) and SSIIM grid (bottom).

The method used for making the Star CCM+ grid is explained in chapter 0. The Star CCM+ grid does not use the transitional zone outlined there. This increases

the risk of errors in the cells close to the inactive area. The Star CCM+ grid also uses an extrusion mesh at the inlet. The extrusion is about 100 meters long. The idea is that the extrusion will allow the velocity field to become more natural before reaching the actual inlet.

6.7 Physics and model assumptions

Both the SSIIM and the Star CCM+ models solve RANS using the finite volume method. Some important characteristics of the models are listed in table 2.

	SSIIM	Star CCM+
Turbulence model	Standard k- ϵ	Realizable k- ϵ
Wall laws	Schlichting	Two layer All- y^+
Discretization scheme	SOU	SOU
Water surface treatment	Adaptive grid	VOF

Table 2: Model setup for SSIIM and Star CCM+, Surna.

The standard k- ϵ model were chosen because it is a widely used turbulence model that have shown good results in many cases for natural rivers and open channels, e.g. Fisher-Antze et al. (2008), R  ther et al. (2010). A Second order upwind discretization was chosen because it is known to give more accurate results than the first order scheme as in R  ther et al. (2010).

The stage-discharge curve (section 6.4.2) was used to get the appropriate discharges and water levels at the inlet and outlet boundaries. In SSIIM the inlet and outlet boundary conditions were set by specifying the appropriate discharge. In Star CCM+ the velocity inlet is used. The water level is then defined together with the velocity at the inlet. The pressure is defined at the outlet as the static pressure due to the water level obtained from the stage-discharge curve. Zero-gradient conditions could not be used at the outlet, due to reversed flow problems in the air phase that caused the solutions to diverge (see section 3.1.3).

For the unsteady simulation, both models used the hydrograph described in section 6.3 as basis for setting the boundary conditions at the inlet. The implementation is however different due to the way the boundaries are set in the two codes. In SSIIM the discharge at inlets must equal the discharge at outlets. Therefore the inlet and outlet discharges in SSIIM were set to rise and sink simultaneously. In Star CCM+ the boundary condition at the inlet were set by keeping the water level constant, and increasing and decreasing the velocities linearly to increase and decrease discharges. At the outlet, the pressure were also defined to increase and decrease linearly. As described in the hydrograph, the discharge is increased from 20 to 80 m³/s during the first 20 minutes, then held steady for 20 minutes, and finally decreased to 20 m³/s during 20 minutes.

A steady state solution at low flow ($20 \text{ m}^3/\text{s}$) was used as the initial condition for the unsteady simulation.

Details on criteria for convergence and steady state conditions for the Star CCM+ model can be found in section 7.8.

7 Modeling Lundesokna

7.1 Background

The results produced by the Surna Star CCM+ model had problems with unphysical velocities in some cells. This is discussed in section 9.4.1.1. The conclusion here was that the necessary grid-fineness to get satisfactory results would require more computational power than was available. When this conclusion was reached it was decided to discontinue the modeling of Surna, and concentrate at modeling a river where good results could be obtained with fewer cells. Lundesokna stood out as good alternative in this respect for several reasons:

- The width to depth ratio is smaller, decreasing the necessary amount of cells for a fine grid.
- The length of the stretch is also shorter than for Surna, further decreasing the cell count.
- A DEM of high quality was already available for a previous SSIIM model of the river stretch.
- Sufficient field data for validating steady flow was available.
- The site had been used for several hydro-peaking tests, providing suitable scenarios for unsteady flow simulations.

Only a Star CCM+ model was developed for Lundesokna. This chapter explains the development of this model.

7.2 Site description



Figure 18: Map overview, Lundesokna (Coordinates are UTM 33N)



Figure 19: Aerial photo, Lundesokna.

The Lundesokna river is one of the rivers studied by CEDREN as a part of the EnviPEAK project. The river originates in Lake Samsjøen and runs into Gaula at Lundamo in Melhus municipality. Three hydro power plants are located in the river. These are Sama, Håen and Sokna, with a total installed capacity of 67,9 MW and a total average annual production of 268 GWh (Store Norske Leksikon, 2009). The modeled area is a bend in the river located close to the center of Lundamo, where the E6 stem road crosses the river. The Sokna hydro power plant has its outlet just upstream of the location.

A map showing the location of the Surna and Lundesokna in Norway can be found on the last page of this thesis (Appendix C).

The river stretch is characterized by a bend. There is an alternating bar type flow pattern often observed in meandering rivers, Tesaker et al. (2010). Shallow banks can be observed on the right side upstream and on the left side downstream of the bend. A scour hole about 1.5 meters deep can be found just downstream of the bend (figure 20). The location of the scour hole is also consistent with theory on meandering rivers, Tesaker et al. (2010). The river bed consists mostly of gravel and cobbles with a mean particle diameter of 6.6 cm. The modeled stretch is approximately 200 meters long and 20 meters wide.

7.3 Hydro-peaking scenario

Several full-scale experiments on hydro-peaking events have been run at the site and documented by a video camera and pressure-loggers. One such event was chosen for simulation. The experiment involves accelerating the turbines of the upstream power plant Sokna from zero to full load. The resulting discharge at the site rises from about 2 m³/s to about 20 m³/s during the 3 minutes of video footage of the event. The aim of the Star CCM+ model is to simulate the unsteady conditions during this event as closely as possible. As field data is available as water surface elevation measurement and ADCP velocity measurement, the focus of the study is simulating flow fields and water surface elevation.

7.4 Data basis

The collection of data for the Lundesokna model was done in connection with the EnviPEAK project and made available for use in this thesis. This section describes the available data, and how it was used.

7.4.1 Bathymetry and Digital elevation model

A DEM was available at CEDREN in advance of this thesis. The geometry data for the DEM was collected by laser scanning the river bed at low flow. According to Ph.D candidate Roser Casas-Mulet (2012) the data were collected during several low flow events in 2010 and 2011. The banks and dry areas of the river bed were surveyed with a TOPCON laser scan obtaining a spacing between points of 0.04 – 0.4 meters. In the remaining wet areas the geometry were collected using differential GPS and total station surveys. Sampling points in the wet areas were collected at 0.5 – 1.5 meter spacing. A DEM was created from the points using interpolation routines in SSIIM. A .stl surface file was then exported for use in Star CCM+. Figure 20 shows a plot of the elevation model.

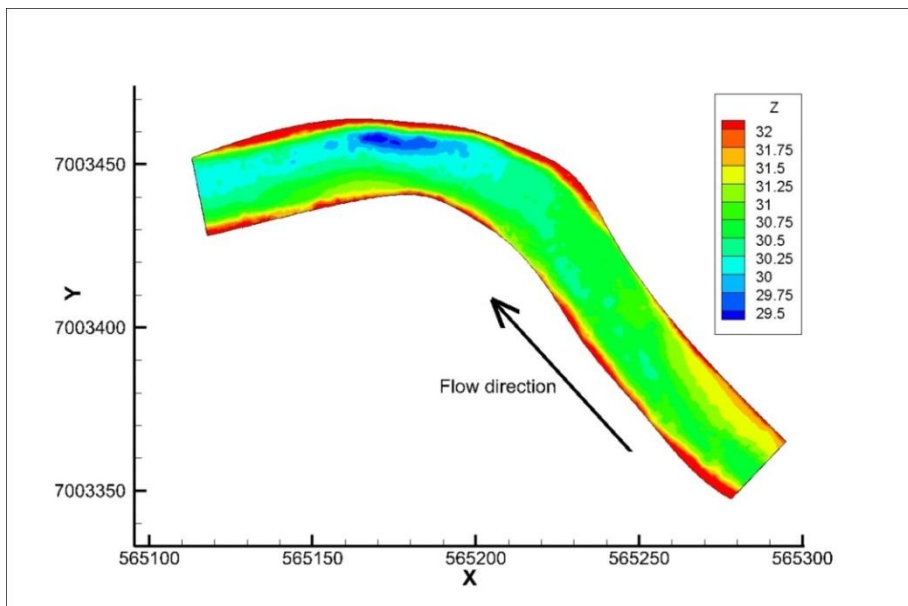


Figure 20: Lundesokna digital elevation model (z = riverbed elevation [m])

7.4.2 Water surface elevation and discharge measurements

Discharge measurements and corresponding water surface elevation measurements at the left bank of the study site were available for discharges 0.43, 0.45, 10.58, 15.31, 16.44, 19.78 and 20.63 m³/s.

Figure 21 shows the water-lines¹ for measured datasets for the highest (20.63 m³/s) and lowest discharge (0.43 m³/s) plotted in ArcGIS. All of these measurements were taken during stationary flow. All water surface elevation measurements used in this project are from the left bank, as indicated in figure 21.

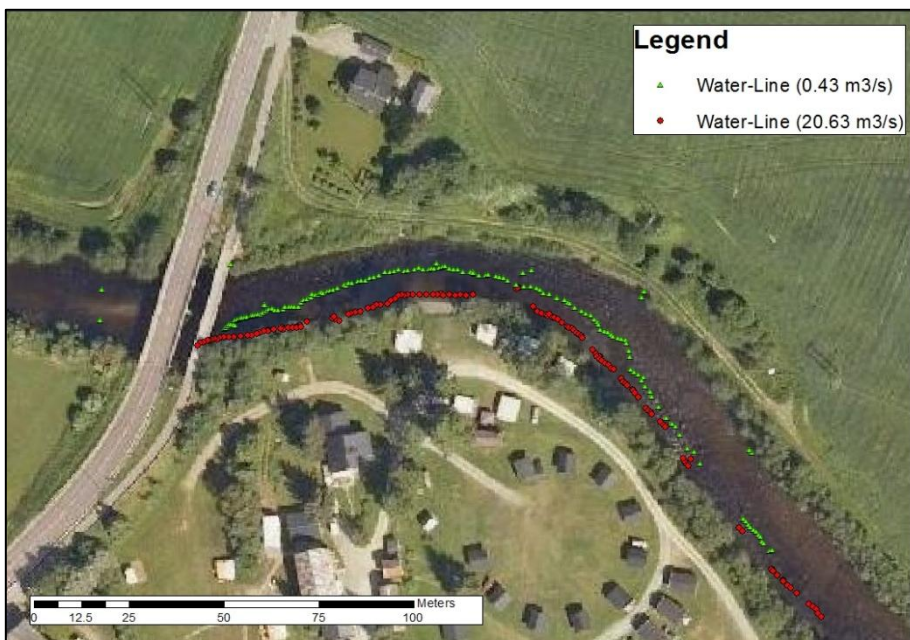


Figure 21: Water-line data plotted in ArcGIS.

The available water surface elevation measurements were used to estimate the stage at the upstream and downstream boundaries of the models. The calculated stages were then used to set boundary conditions at the inlet and outlet (section 7.8). First the data were separated into an upstream and a

¹ In this thesis the term “water-line” is used, meaning the line where river and bank meets. Water surface elevation measurements are collected at the water-line. Where these measurements are plotted in the plane this term is used to avoid confusion with water surface profiles.

downstream section, as shown in figure 22. Then linear regression was used to estimate the upstream and downstream stage. The data were used to make a stage-discharge curve. Table 3 show data from the stage-discharge curve for various discharges.

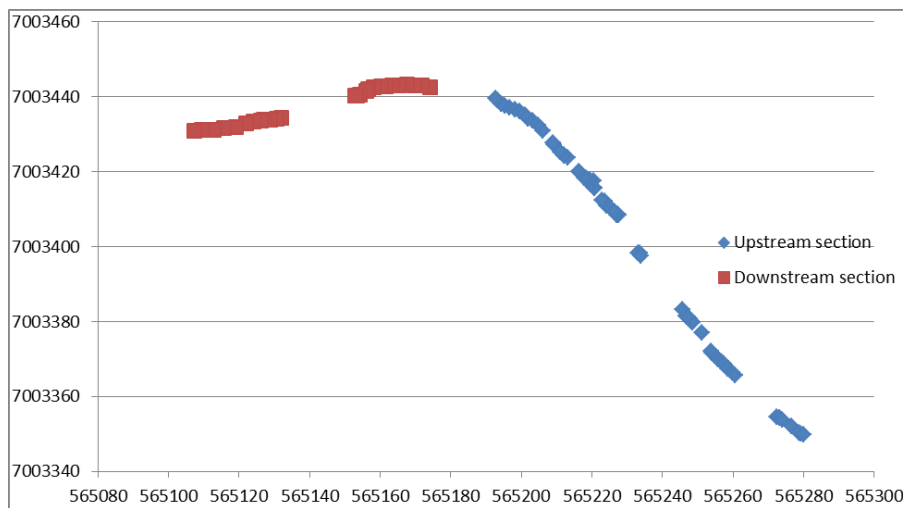


Figure 22: Plot showing water lines. The data is split into an upstream and downstream section.

<i>Stage-discharge table</i>		
Discharge [m^3/s]	Downstream stage [m]	Upstream stage [m]
0	30.36	31.12
2	30.42	31.17
4	30.48	31.22
6	30.54	31.28
8	30.61	31.33
10	30.67	31.39
12	30.73	31.44
14	30.79	31.50
16	30.86	31.55
18	30.92	31.60
20	30.98	31.66

Table 3: Stage-discharge table for Lundesokna.

7.4.3 *Velocity measurements*

Field ADCP measurements of the velocity in 12 transects just downstream of the bend were available from EnviPEAK. The velocity was measured by dragging a floater equipped with the ADCP equipment across the river. More details on ADCP measurements in rivers can be found in the preliminary project (Pedersen, 2012a).

The measurements were collected at discharges around $20 \text{ m}^3/\text{s}$. The individual transects are plotted in figure 23 to show the spread of the data. As seen in the figure, the transects are arcs rather than straight lines. This is due to difficulties with keeping the floater steady in the stream.

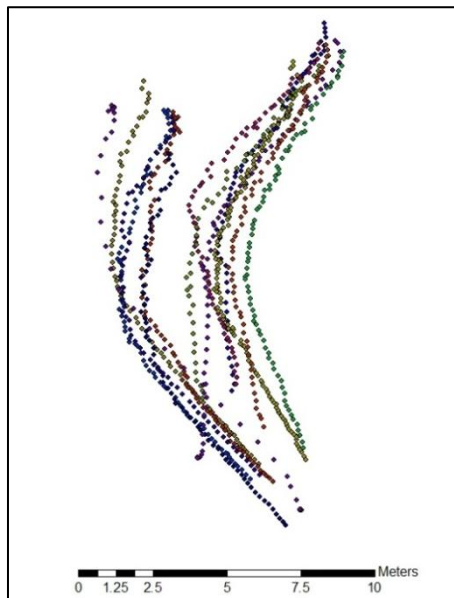


Figure 23: Plot of individual transects

The velocity data was treated by a series of scripts developed by MSc student Åsmund Hasaas and Ph.D candidate Hanne Nøvik at the department for hydraulic and environmental engineering. Details can be found in Hasaas (2011). The main idea of the script is to project all the transect arcs onto a cross-section and then average the velocities. This is illustrated in figure 24. The velocity measurements were used to validate the Star CCM+ steady flow simulations at $20 \text{ m}^3/\text{s}$ (section 8.2.2).



Figure 24: Average transect and projected cross section plane.

7.4.4 Field data from the hydro-peaking event

3 minutes of video footage exist for the hydro-peaking event. The video camera was placed just downstream of the bend on the right bank, and filmed towards the bend upstream. The video is provided as a digital attachment (Appendix A). The video data were used as basis for the unsteady scenario. The results from the unsteady simulations in Star CCM+ were compared to the video footage (section 8.2.3). Figure 25 shows a snapshot from the video.



Figure 25: Snapshot from the video of the hydropeaking event.

Pressure logger data with a 2 minute resolution was available from the hydropeaking event. The resolution of the logger data is unfortunately too coarse to be used for validation of the unsteady simulations, as the whole event happens during 2 – 3 minutes.

7.4.5 Sediment data

Sediment data for the substrate was available for the sampling spots shown in figure 26. The data were used to estimate the roughness height parameter in the model by averaging all the points. The mean grain size is 0.066 m and the d_{90} parameter is 0.138 m. Van Rijn's empirical formula (Van Rijn, 1984) then gives $k_s = 3d_{90} = 0.41$ m. This is a very rough estimate, and the roughness height must be calibrated for use in the model.

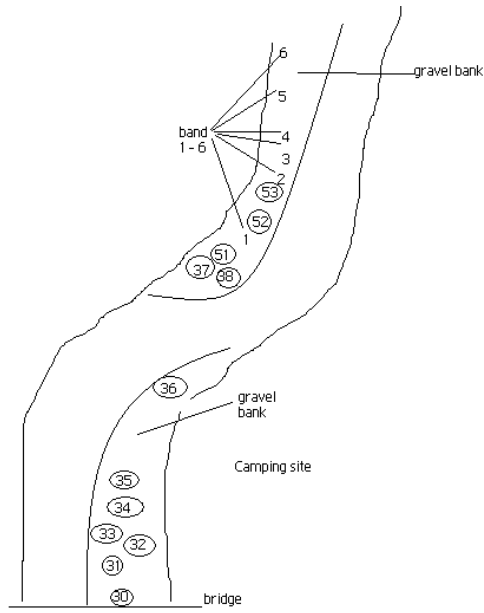


Figure 26: Sketch showing sediment sampling points, Lundesokna

7.5 Grid sensitivity tests

A criterion for a good grid is that the solution does not differ significantly when applying a finer grid. A range of grids with varying fineness was tested to find the optimum grid for the Lundesokna case. The tested grids are summarized in Table 4. The percentages are cell sizes as percentage of the base size. For the prism layer this indicates the sum of the thicknesses for all the layers. The grid designs were based on experience gathered from the grid experiments done for Surna and the principles described in chapter 5.

<i>Name</i>	<i>Cell count</i>	<i>Base size</i>	<i>Prism layer</i>	<i>Active Area Refinement</i>
m1	650,254	0.5 m	Two layers, 33%	None
m2	366,174	0.5 m	None	Vertical: 50% (0.25 m)
m3	1,536,071	0.5 m	None	Horizontal: 50% (0.25 m) Vertical: 25% (0.125 m)
m4	2,239,913	0.8 m	Two layers, 15%	Horizontal: 50% (0.4 m) Vertical: 25% (0.2 m) Special refinement at bend: (Horizontal 25%, Vertical 15%)
m5	1,250,867	0.7 m	Three layers, 15%	Horizontal: 50% (0.35) Vertical: 25% (0.175)

Table 4: Overview over tested grids, Lundesokna

The initial tests were done with grid m1 to m4 at $4 \text{ m}^3/\text{s}$ discharge. The comparison was done by inspecting the surface velocity vector fields of the different simulations. Results from the $4 \text{ m}^3/\text{s}$ tests can be found in Appendix B. The conclusions from the tests were that some aspects of the complex flow around the bend were only modeled properly by the m3 and m4 grids. The m3 grid lacks a prism layer, which was thought necessary to capture the water surface at low flows, and m4 has a too high cell count. Because of this the m5 grid was made, with three prism layers to be sure to capture low flows well enough, and slightly courser cells than m3. Tests results for the m5 grid were considered satisfactory, and the grid was then chosen for use in calibration tests. After the calibration process the m5 grid was modified. The modified grid (m6) and another finer grid (m7) are described in section 7.7.

7.6 Calibration of the model

In order to obtain the proper sand-equivalent roughness height parameter (k_s) for the simulation the model was calibrated against the measured water line at 16.44 m³/s discharge. As mentioned in section 2.6.1 it does not make physical sense for the roughness height to be larger than the normal distance from the bed to the cell-centroid of the bed-cell. This introduces the problem that it is desirable to have small cell-heights close to the bed in order to properly model the bed and resolve the water surface using the VOF method, while it at the same time is necessary to have larger cells to set correct roughness values. This problem is further discussed in section 9.3. The original grid (m5) chosen during the grid tests has a prism layer with vertical cell size of approximately 0.1 meters close to the bed. This means that the maximum possible roughness height is 0.05 meters. The estimate based on sediment data, however, was 0.41 meters! For the calibration, two new grids were made which are identical to the m5 grid except for the prism layer. The prism layer in the new grids has vertical cell sizes of 0.2 and 0.3 meters to allow roughness heights of 0.1 and 0.15 meters respectively. In Star CCM+ the walls can be modeled as rough or smooth. The rough wall setting uses the roughness height as input. For reference a simulation with the wall setting set to smooth was also run.

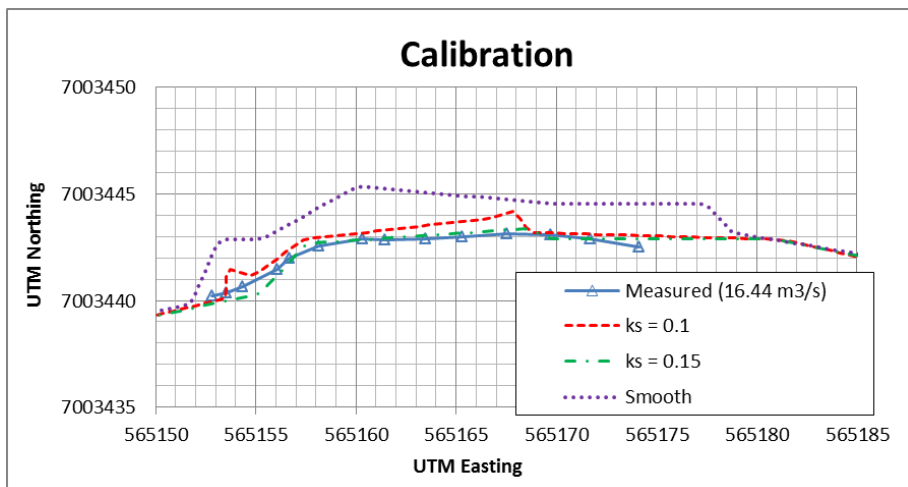


Figure 27: Top-down plot of water-lines with varying roughness height close to the bend.

Figure 27 shows a top-down plot of the resulting simulated water lines and water lines at the bank just downstream of the bend. As the figure indicates, the

simulations with roughness height 0.1 and 0.15 meters shows a much better fit with the measured values compared to using a smooth surface model. This is as expected, as the sand and gravel that makes up the river bottom is a rough surface. Further, 0.15 meters seem to give a better fit than 0.1. As a 0.3 meter prism layer is assumed to be too coarse for the VOF method to work properly a grid with a prism layer of 0.175 meters was used as a compromise. The grid is designated m6 and characteristics of the grid is listed in Table 5. Further discussion on the low roughness value used can be found in section 9.3.

7.7 Characteristics of the final grids

The grids were made using active area refinements as described in chapter 5. On the basis of the stage-discharge curve obtained from the water surface elevation measurements the upstream stage has a elevation of 31.66 meters at maximum discharge ($20 \text{ m}^3/\text{s}$). The active area was defined as all cells with a vertical elevation lower than 32 meters to avoid water fractions in the inactive area.

The final grids used for simulations in Surna are presented in table 5:

	m6-grid	m7-grid
Cell count:	855,837	3,091,108
Cell type:	Trimmer mesher	Trimmer mesher
Passive area cell size	0.7 meters	1.6 meters
Active area refinement cell size	Horizontal: 0.35 meters Vertical: 0.175 meters	Horizontal: 0.2 meters Vertical: 0.1 meters
Prism layer	One layer, 0.175 meters	One layer, 0.1 meters

Table 5: Grids used for modeling Lundesokna

The m6 grid is equal to the m5 grid (section 7.5) except that the size of the prism layer has been adjusted due to the results from the calibration (section 7.6).

Both the m6 and the m7 grid are based on the methods described in chapter 5.

The m6 grid was used for both the steady flow simulations and the unsteady flow. The m7 grid was primarily used for running the unsteady flow simulations.

Cross section views of the grids are presented in Figure 28.

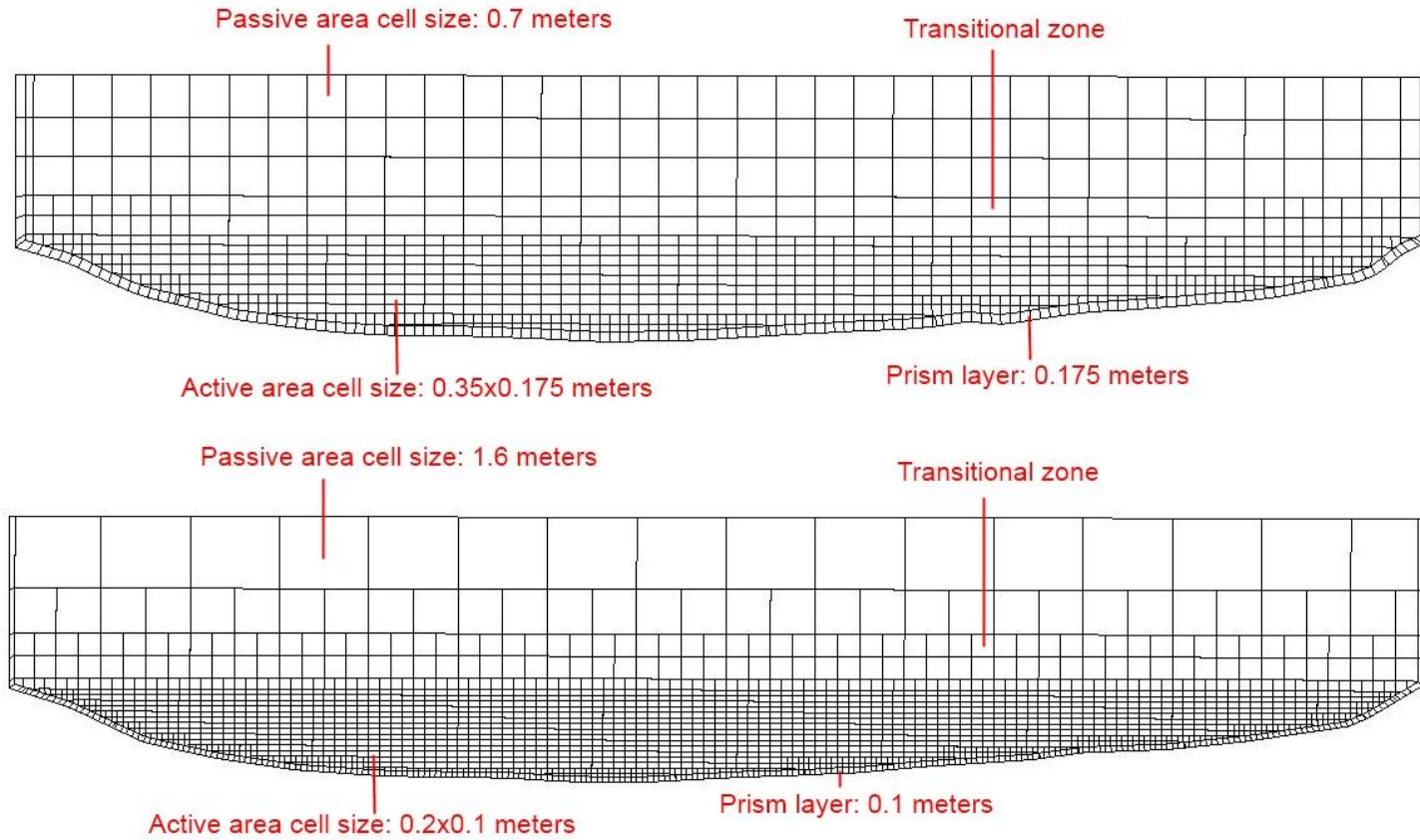


Figure 28: Cross section view for Lundesokna grids. Top: m6 grid. Bottom: m7 grid

7.8 Physics and model assumptions

The model setup used is similar to that of the Star CCM+ Surna model and is summarized in table 6. More details on numerical modeling methods can be found in chapter 2 and 3.

Star CCM+ model setup	
Turbulence model	Realizable k-ε
Wall laws	Two layer All-y+
Discretization scheme	SOU
Water surface treatment	VOF

Table 6: Model setup for Star CCM+, Lundesokna.

The solution domain is bounded by several boundary types. A wall-boundary is used for the bed and sides. Here the roughness height must be set as an input parameter (section 2.6.1). The lid is modeled as a pressure outlet with atmospheric pressure set as a boundary condition. The upstream boundary is a velocity inlet. In addition to setting the velocity, the water level is set as a boundary condition. The water level is set as a constant depending on the discharge and is found by the stage-discharge table (table 3). The velocity is assumed to be uniform for the inlet cross-section. At the outlet boundary the pressure is defined by the downstream water level. For steady flow this is a constant retrieved from Table 3. For unsteady flow the water level is modeled as:

$$z = z_{low} + \frac{z_{high} - z_{low}}{t_{max}} t \text{ for } 0 < t \leq t_{max}$$

$$z = z_{low} \text{ for } t < 0$$

$$z = z_{high} \text{ for } t > t_{max}$$

Where z_{low} is the water level for the initial (low) discharge, z_{high} is the water level for the maximum discharge, t is the time from the water reaches the downstream outlet, and t_{max} is the time when the high discharge have been reached at the outlet. t_{max} was set to 100 seconds based on observations in the video and test simulations.

For steady flow simulations the water level and pressure in the solution domain is set equal to the values at the outlet as an initial condition. This is to avoid instabilities experienced with having inflow at the outlet due to the pressure at the boundary being higher than the pressure in the cells upstream. As described in more detail in section 3.1.3 negative flow at pressure boundaries is undesirable. The

steady flow simulations are run by first “filling up” up the model. This means that the flow is unsteady for a number of iterations, before the wave caused by the discharge at the upstream boundary hits the downstream boundary and the flow stabilizes to steady flow conditions. The steady flow simulations were run until mass balance was reached for the solution domain, meaning that $Q_{\text{inlet}} = Q_{\text{outlet}}$. A plot of the mass flows (kg/s) for the $16.44 \text{ m}^3/\text{s}$ simulation is shown in Figure 29. The initial negative outflow at the outlet is caused by the pressure boundary condition at the outlet, but is dampened considerably by the initial condition in the solution domain described above. In this case, the wave reaches the outlet in about 3600 iterations, corresponding to 90 seconds physical time. The wave top reaches the outlet at about 8000 iterations (200 seconds), and then the wave flattens out and stationary conditions are reached at about 20000 - 24000 iterations (500 – 600 seconds).

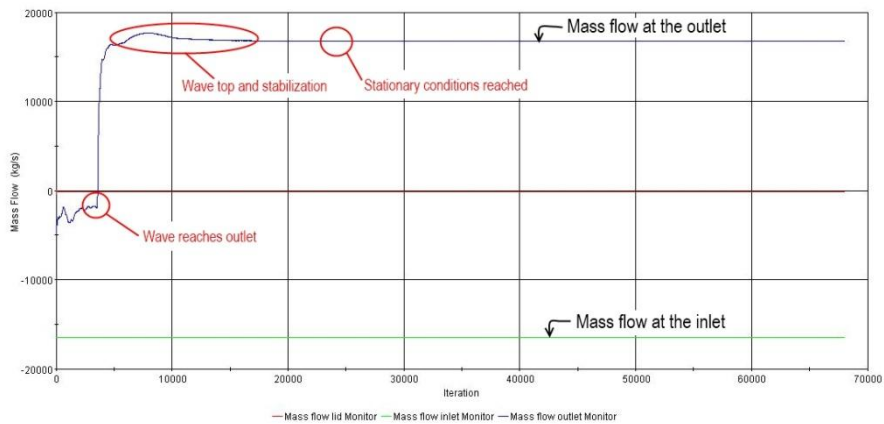


Figure 29: Mass balance plot for stationary simulation at $16.44 \text{ m}^3/\text{s}$ Results

Convergence of the simulations was also assessed. A plot of the residuals from a simulation can be seen in figure 30. Two observations can be made:

- The periodic fluctuations of the plot indicate the convergence of the inner iterations during a time step.
- When averaging these the convergence of the time-step iterations is observed.

An indication of convergence is the drop of residuals during the inner iterations. In figure 30 the water variable drops by approximately one order of magnitude during a time-step. That the plot globally first drops and then stabilizes is also an indication of convergence in Star CCM+. The simulations were assumed to have satisfactory convergence if the water variable dropped by one order of magnitude and the plot generally dropped and stabilized.

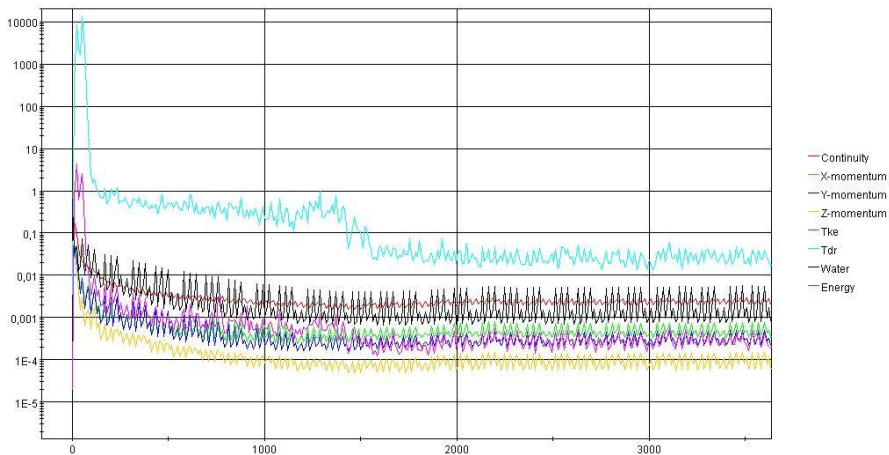


Figure 30: Residual plot in Star CCM+

For the unsteady flow simulation the same procedure as for steady flow is followed, so that stationary conditions are reached for the low flow. This then becomes the initial conditions for this simulation. The water level and velocity boundary conditions at the inlet are then increased to reflect the high flow. It is assumed that the increase is instantaneous at the inlet. In reality the acceleration of a turbine from zero to full load may take from about 6-10 seconds and the power plant outlet is about 1 kilometer upstream of the plant, which will cause some diffusion of the wave. It is however assumed that these conditions do not significantly contribute to the solution close to the outlet.

8 Results

8.1 Surna

8.1.1 Steady flow results

Steady flow simulation results for SSIIM were available from the preliminary project (Pedersen, 2012a). The results from steady flow simulations in Star CCM+ are presented here together with the results from SSIIM for comparison.

Physical assumptions used in the models are described in section 6.7, and the grids used are presented in section 6.6. All the simulations were run at $48.46 \text{ m}^3/\text{s}$ discharge.

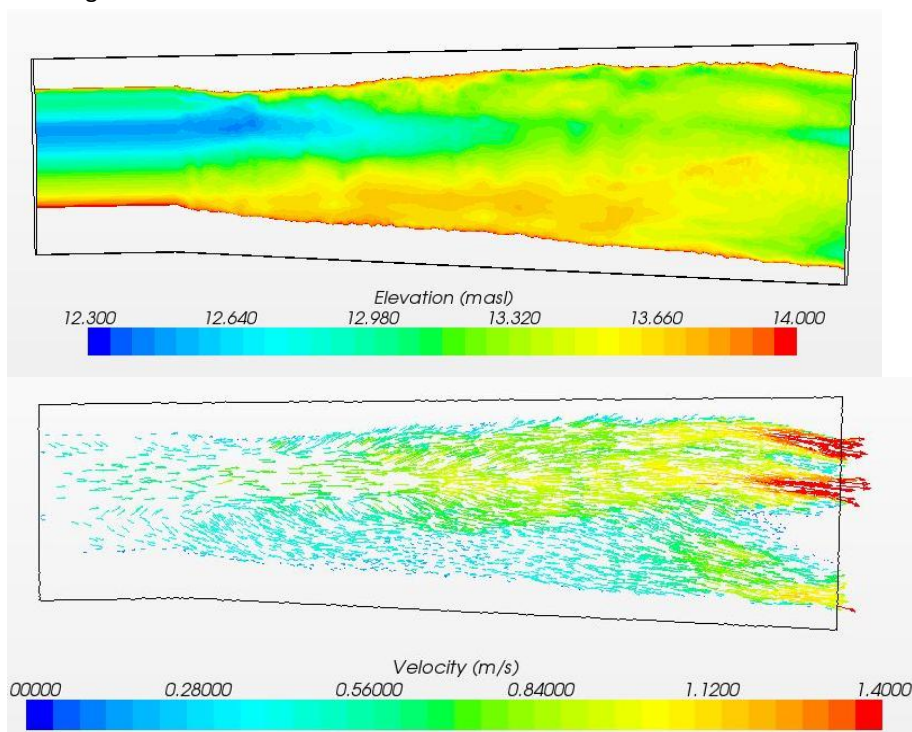


Figure 31.: River bed elevation [m] (upper), and surface velocity vectors [m/s] (lower) for the Star CCM+ model, steady flow, Surna

Figure 31 shows a plot of the surface velocity vectors for the Star CCM+ steady simulation together with a plot of the bed elevation levels. As seen from figure 31 Star CCM+ was predicting the highest velocities in two distinct streams at left side of the island close to the outlet. Some cross stream occurred in the shallow area in the

middle by the outlet, and a high-velocity stream was present at the right side of the island. Upstream the velocities were higher on the left side in the deep part. In general low velocities were found in the shallow bank on the right side. As seen in figure 32 the flow pattern in Star CCM+ is comparable to the flow pattern in the SSIIM model from the preliminary project (2012a).

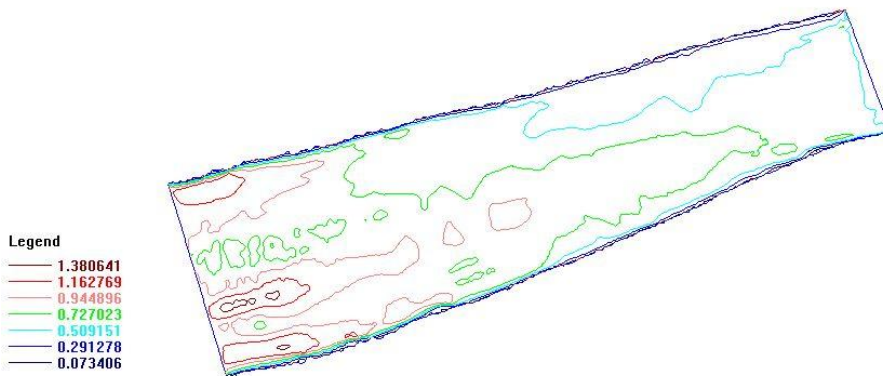


Figure 32: Surface velocity magnitudes [m/s] form SSIIM, steady flow, Surna.

Figure 33 shows a plot of the bed shear forces in both models. Both simulations report the highest shear forces in the main streams on the left side of the island, close to the outlet boundary, but the Star CCM+ model predicts higher shear forces here. There is a smaller peak at the right side of the island. Here, the SSIIM model predicts slightly higher shear forces. In general the Star CCM+ model predicts higher shear forces further upstream.

Note that the Star CCM+ model also shows “dots” of higher shear forces that are not present in the SSIIM model. This effect is better seen in the unsteady simulation results (Figure 36). These dots are likely due to unphysical velocities in some of the cells in Star CCM+. This is further discussed in section 9.4.1.1..

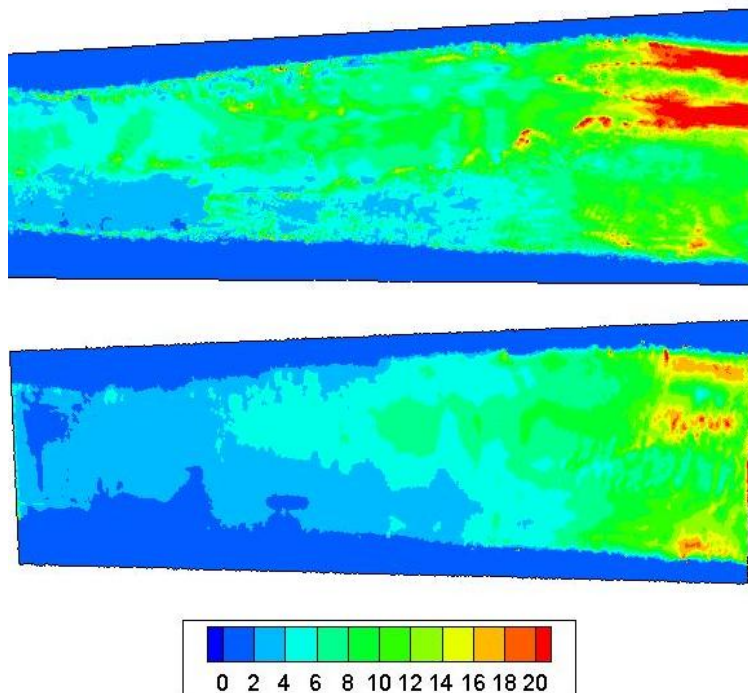


Figure 33: Comparison of bed shear [Pa] in Star CCM+ (upper) and SSIIM (lower), steady flow, Surna.

Average velocity profiles were extracted in a cross section (figure 34) in Star CCM+ and SSIIM. The resulting plot is presented in figure 35. As shown, the general tendency and position of the local velocity maximum is in agreement. The maximum velocity in Star CCM+ was 0.94 m/s, while the maximum was 0.74 m/s in SSIIM. From 80 – 110 meters measured from the left bank the difference in velocities is about 0.3 m/s. Generally SSIIM produces a smoother velocity profile with a lower peak, while Star CCM+ predicts sharp gradients in several places. The root-mean-square deviation (RMSD) is 0.16 m/s and the normalized RMSD is 17.74 %.

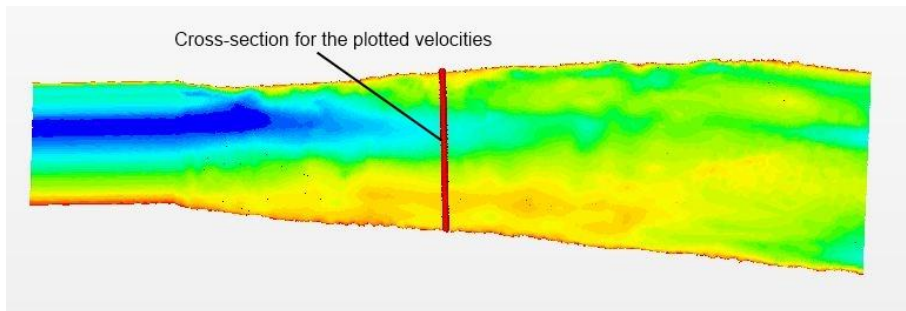


Figure 34: Position of the cross-section for extracting velocities

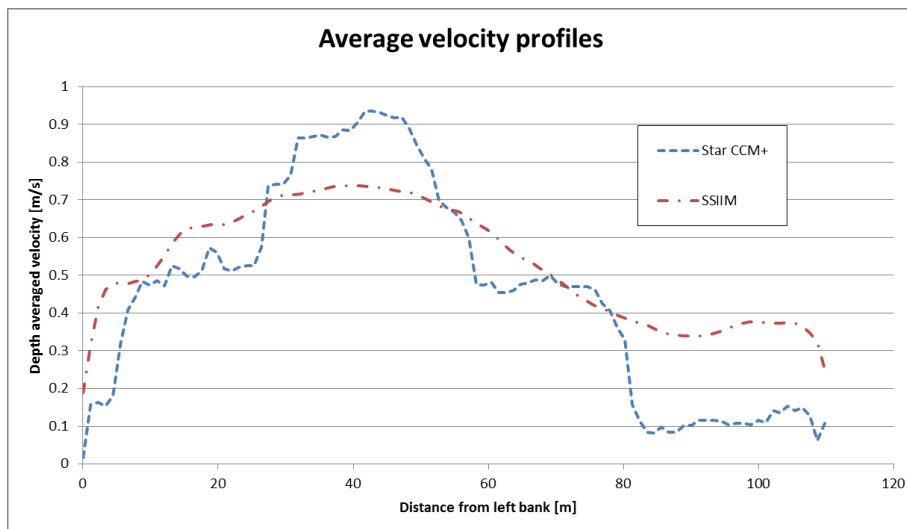


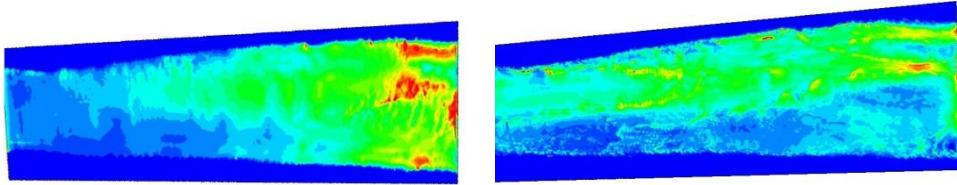
Figure 35: Average velocities in a cross-section [m/s], steady flow, Surna

8.1.2 Unsteady flow results

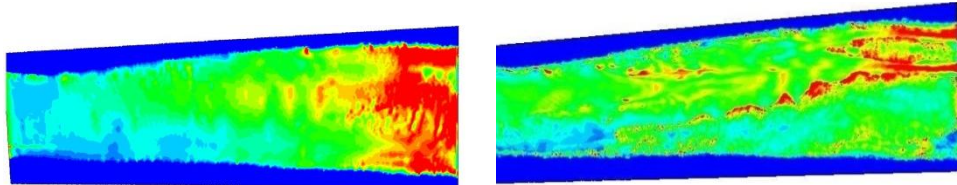
Unsteady flow was simulated on basis of the hydro peaking scenario described in section 6.3. The resulting shear forces for SSIIM and Star CCM+ is presented here.

The physics setup and grids used for Star CCM+ were the same as for steady flow, described in section 6.6 and 6.7. The minimum discharge was $20 \text{ m}^3/\text{s}$ and the maximum was $80 \text{ m}^3/\text{s}$. The discharge was raised during 20 minutes, held steady at maximum for 20 minutes and then lowered for 20 minutes.

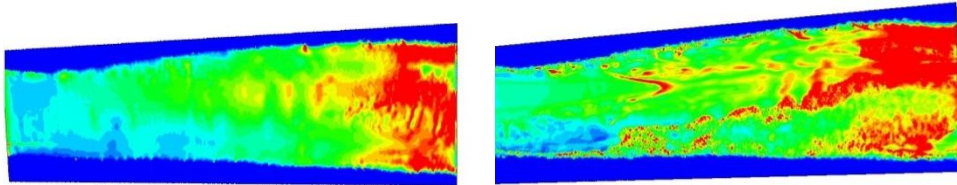
Resulting shear forces for 10, 20, 30, 50 and 60 minutes are plotted in figure 36. The figure shows that peak shear forces at the outlet were reached after about 20 minutes in the SSIIM model and after 30 minutes in the Star CCM+ model. This is due to the quasi-unsteady approach in SSIIM (section 3.2.2). When accounting for the lag in water travel time in the Star CCM+ model, the two models shows similar peak shear forces at the boundary (comparing figure 36 b and c for SSIIM with figure 36 c and d for Star CCM+). The Star CCM+ model however predicts somewhat higher peak velocities, and also “dots” of high shear forces are shown. These were likely due to unphysical velocities as discussed in section 9.4.1.1.

Bed Shear-force plot [Pa] Left: SSIIM, Right: Star CCM+

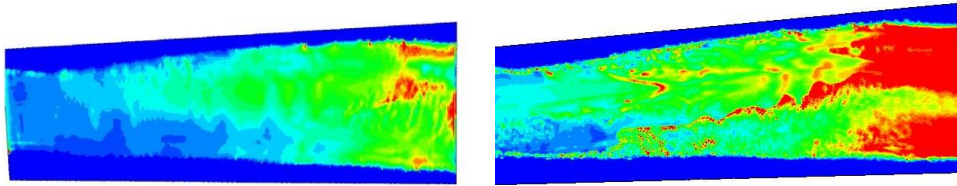
a) 10 minutes



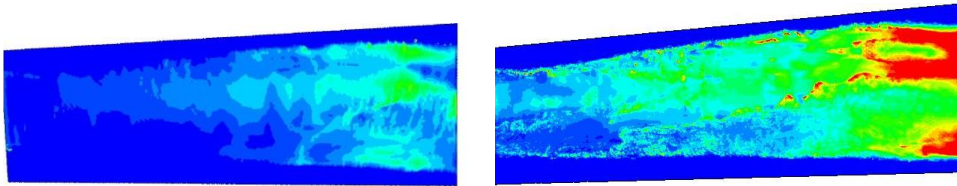
b) 20 minutes



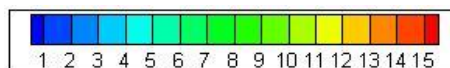
c) 30 minutes



d) 50 minutes



e) 60 minutes

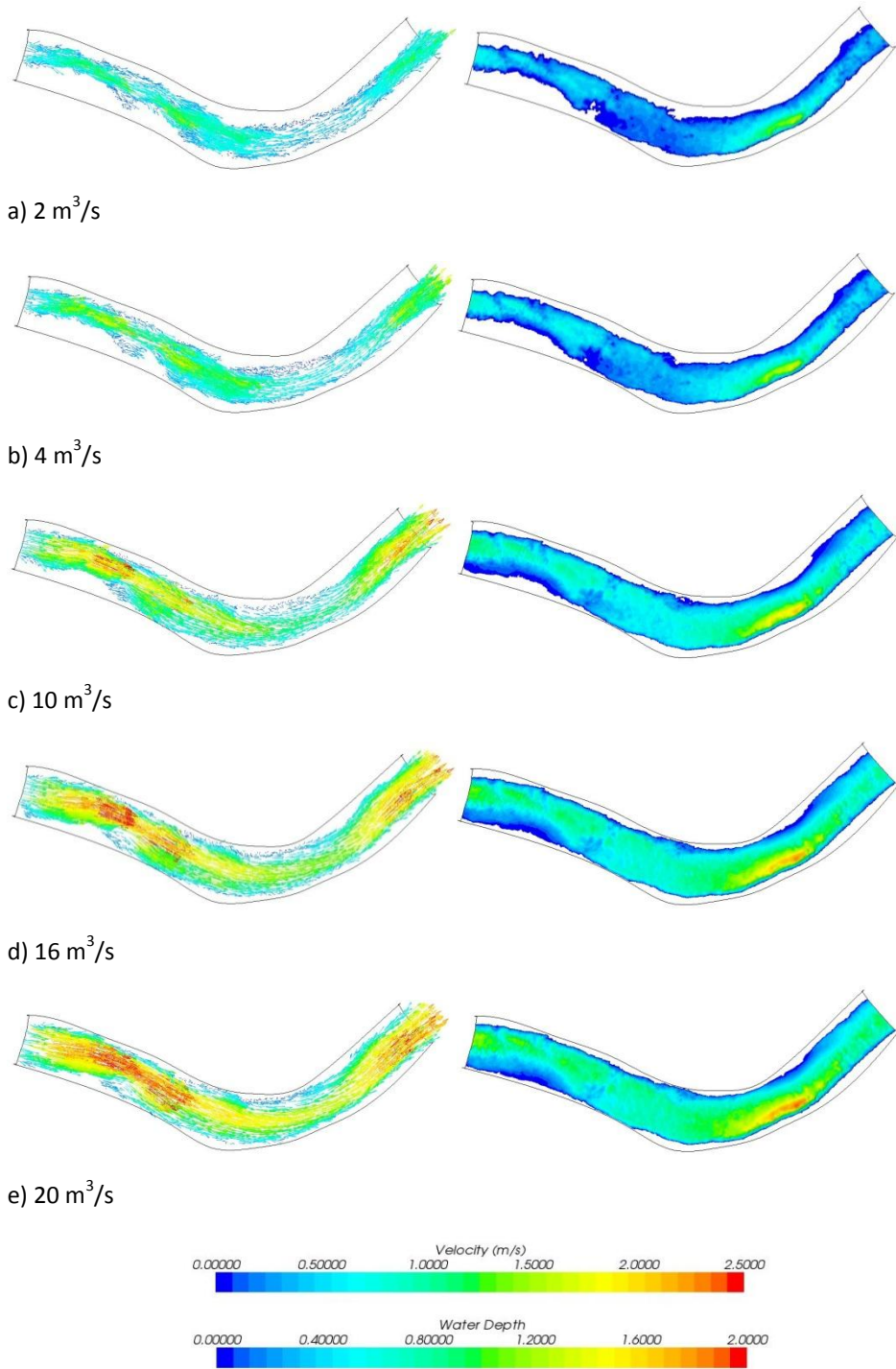
**Figure 36: Bed shear force [Pa] , Left: SSIIM, Right: Star CCM+, unsteady flow, Surna**

8.2 Lundesokna

8.2.1 *Steady flow results*

Steady flow simulations were run at 2, 4, 10.58, 16.44 and 20 m³/s. All of the simulations were run on the m6 grid described in section 7.7. The physics setup used is described in section 7.8.

Figure 37 shows a surface velocity plot and water depth plot of the steady simulations. The velocity plot indicates lower velocities in the area close to the bend, where the water is deeper. The main stream alternates from the left side of the channel upstream to the right side just downstream of the bend. Zones with stagnation or very low velocities were formed in the shade of the upstream bank on the right side, and in the shade of the bend. No major changes in flow pattern, except for an increase in velocity, were seen for increasing discharges.

Steady simulation results. Left: Velocity vectors. Right: Water depth**Figure 37: Left: Surface-velocity vector [m/s]. Right: Water depths [m], steady flow, Lundesokna**

8.2.2 Steady flow validation

Two types of field data were available for validating the steady flow results. Firstly coupled water surface elevation and discharge measurements were available at 10.58, 16.44 and 20.63 m³/s discharges (section 7.4.2). Secondly velocity measurements by ADCP were available for a cross section at approximately 20 m³/s discharge (section 7.4.3).

Figure 38 to figure 40 show top-down plots of the water-line at 10.58, 16.44 and 20 m³/s discharges close to the bend. The water surface elevation field measurements at 16.44 m³/s discharge was used for calibrating the model (section 7.6).

As mentioned in section 7.6 some under-prediction of the water-lines was to be expected due to the low roughness height value. However, the simulations at 10.58 m³/s and 20.63 m³/s actually shows better agreement with the field data compared to the 16.44 m³/s simulation, and the water line does not seem to be under-predicted in these simulations. This is further discussed in section 9.3.

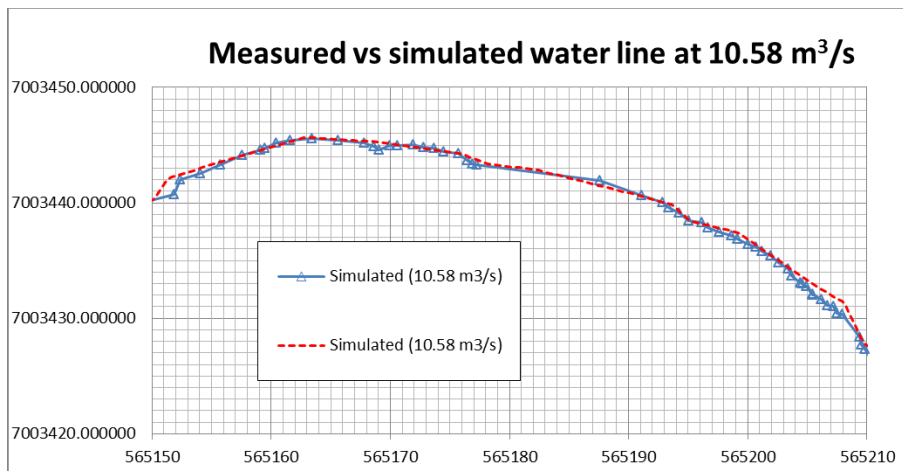


Figure 38: Top-down plot of simulated versus measured water-lines at 10.58 m³/s, steady flow, Lundesokna

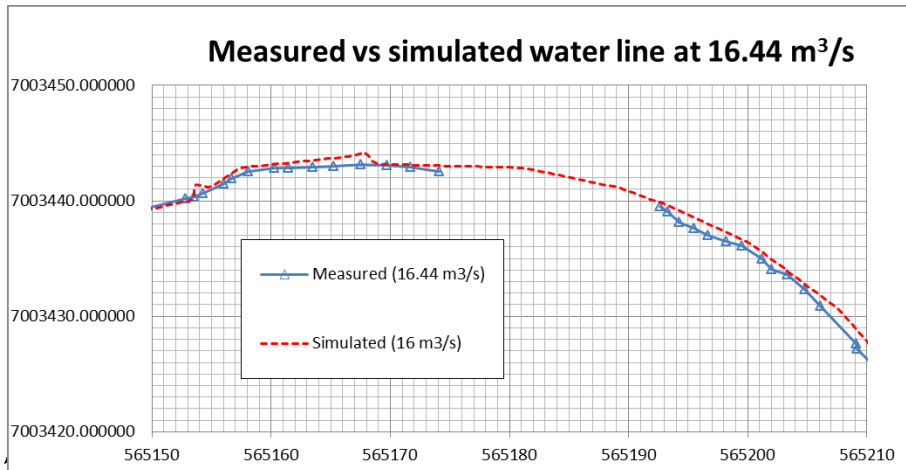


Figure 39: Top-down plot of simulated versus measured water-lines at 16.44 m³/s, steady flow, Lundesokna

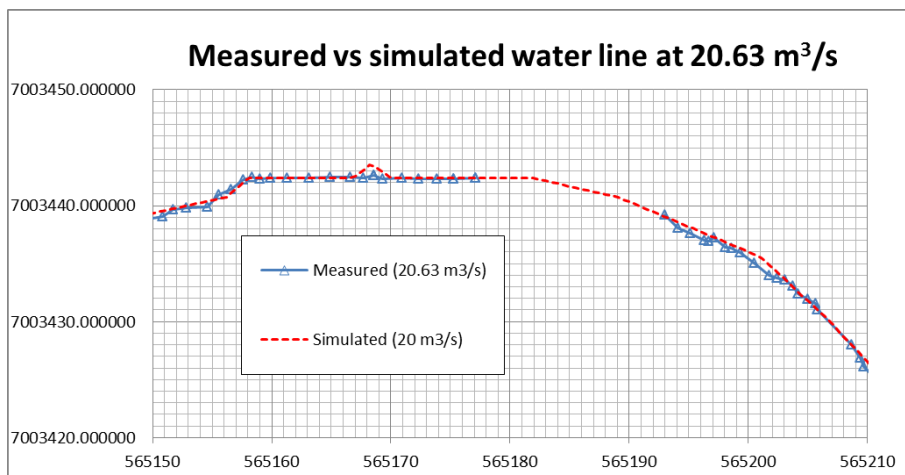


Figure 40: Top-down plot of simulated versus measured water-lines at 20.63 m³/s, steady flow, Lundesokna

ADCP field velocity measurements were available for a discharge of approximately $20 \text{ m}^3/\text{s}$ (section 7.4.3). Figure 41 shows plots of the measured and simulated velocities in a cross-section. The depth averaged velocity profiles in the same cross section are also shown. The maximum depth-averaged velocity measured in the field was 1.34 m/s while the prediction by the Star CCM+ simulation was 1.38 m/s . Both the simulation and the field data show peaking velocities between 4 and 6 meters from the right bank. Comparing the measured to the simulated data the root-mean-square deviation (RMSD) is 0.13 m/s and the normalized RMSD is 9.38% . In general the velocities close to the left bank was slightly under-predicted by the Star CCM+ model, while the peak velocities and velocities close to the right bank were over-predicted.

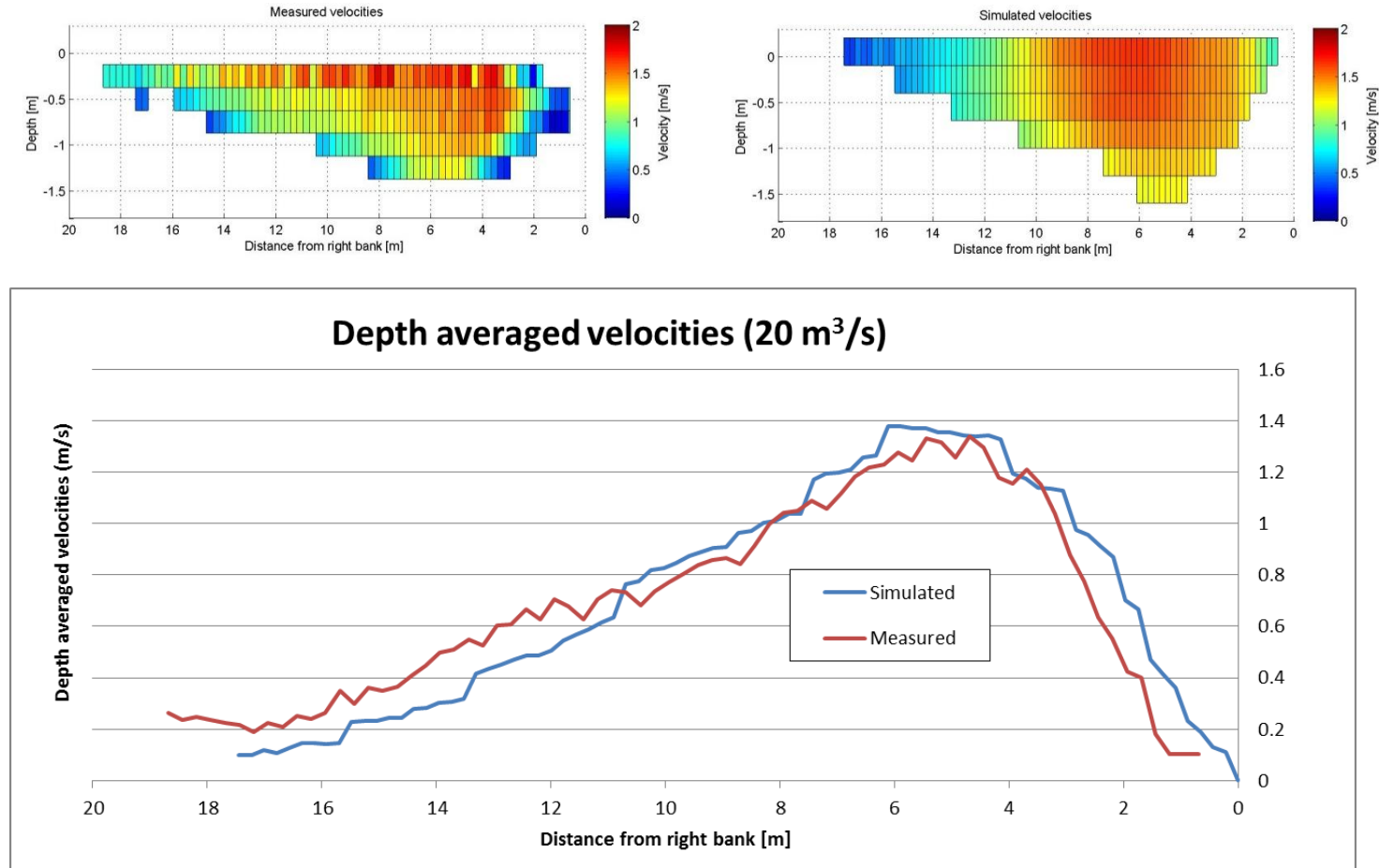


Figure 41: Measured velocities (top left) and simulated velocities (top right) in a cross-section. Depth averaged velocity profiles [m/s] (bottom), steady flow, Lundesokna

8.2.2.1 *Grid sensitivity*

The finer m7 grid was only used to run the unsteady simulation. However, steady state solutions were extracted for $2 \text{ m}^3/\text{s}$ and $20 \text{ m}^3/\text{s}$ at the start and end of the simulation. The solution data was used to test the grid sensitivity of the m6 grid for the steady state simulations.

A comparison of surface velocity vector plots is shown in

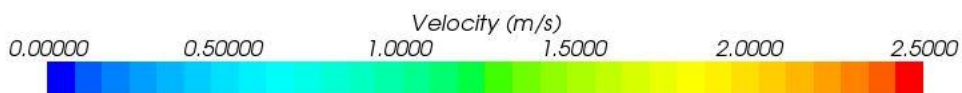


figure 42 and figure 43. The results are discussed in section 9.5.1.

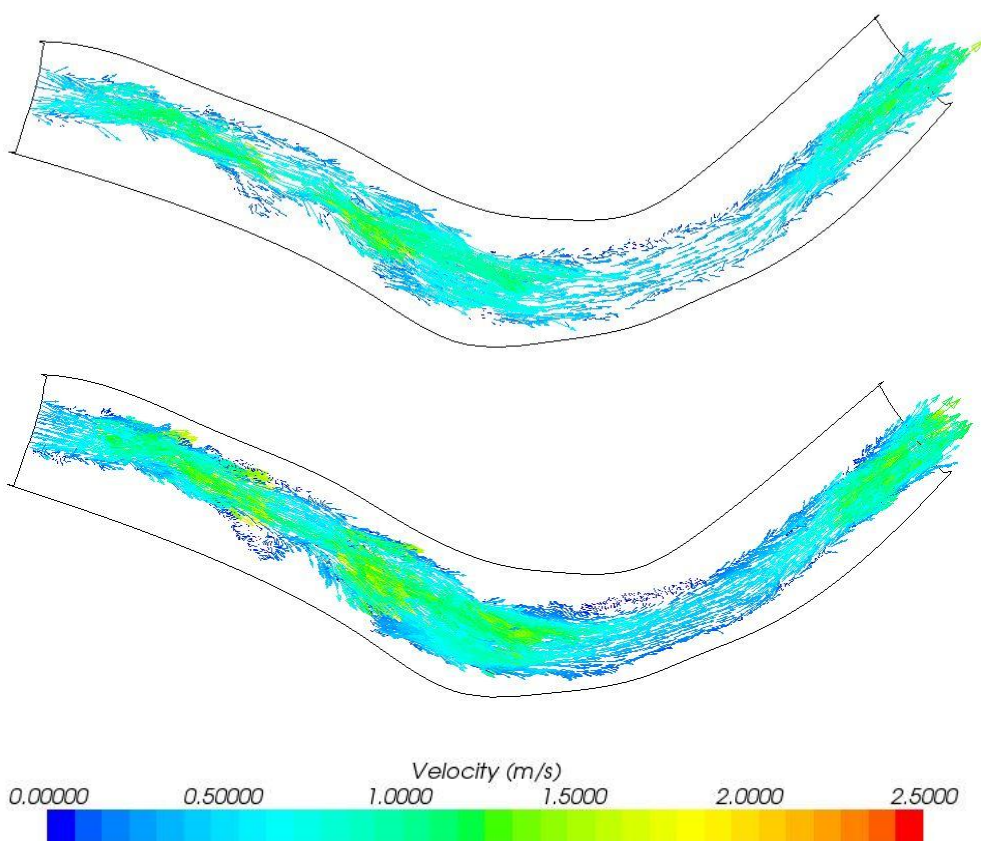


Figure 42: Comparison of surface velocity vectors at $2 \text{ m}^3/\text{s}$. Top: m6 grid. Bottom: m7 grid, steady flow, Lundesokna

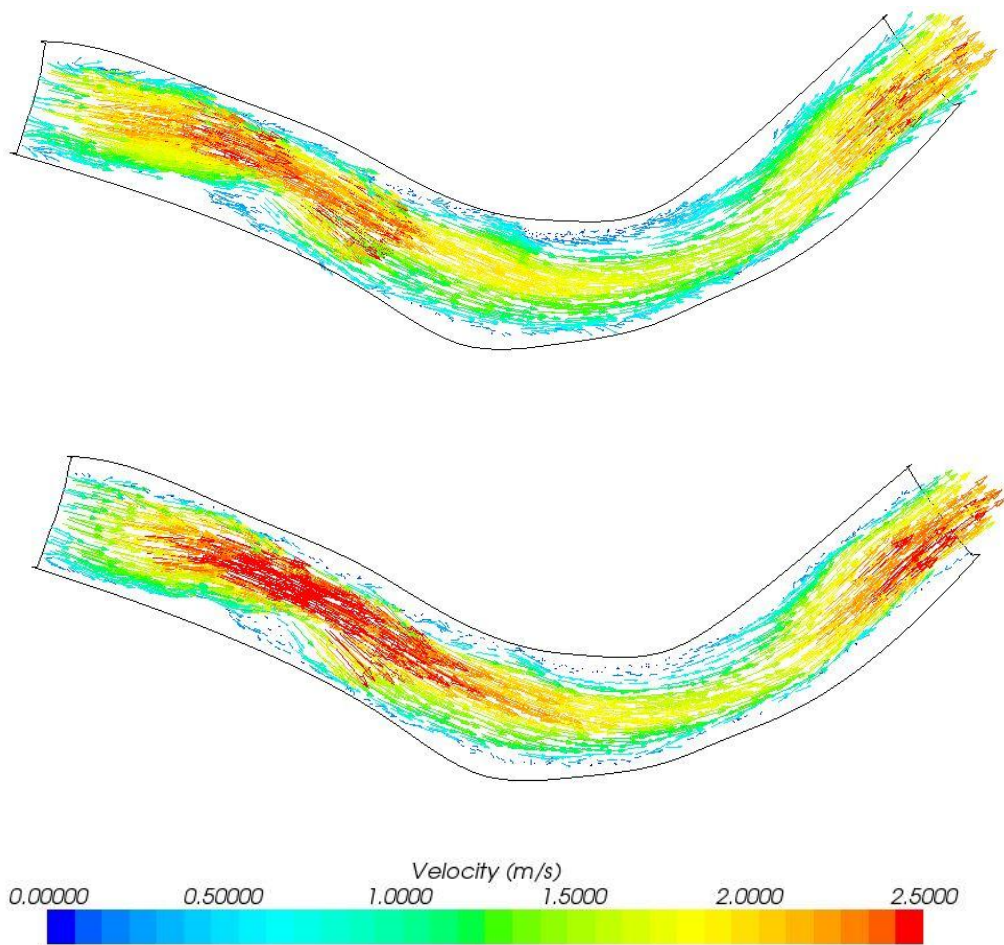


Figure 43 Comparison of surface velocity vectors at $2 \text{ m}^3/\text{s}$. Top: m6 grid. Bottom: m7 grid, steady flow, Lundesokna

8.2.3 Unsteady flow results

The unsteady simulations were run on both the m6 and the m7 grid. The grids are described in section 7.7. Physics model set up are described in section 7.8. As the m7 grid is finest, the results from that grid are presented here.

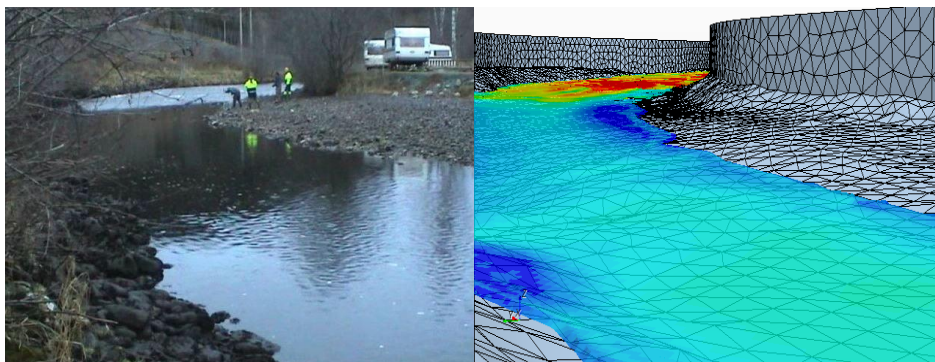
A scene in Star CCM+ was staged to resemble the Hydro-peaking video. Scenes were extracted as pictures every 0.1 seconds, physical time, and a video was made from the exported pictures. Plots of water depth and surface velocity vectors were also extracted and similarly treated. The videos are available as digital attachments for the m7 grid. A video of the staged scene on the m6 grid is also available (Appendix A).

Figure 44 shows comparisons of the hydro-peaking video and the simulated scene. The simulated scene shows velocity magnitudes on a semi-transparent water surface. The times are given from the start of the unsteady simulation. Times in parenthesis correspond to the time in the hydro-peaking video file.

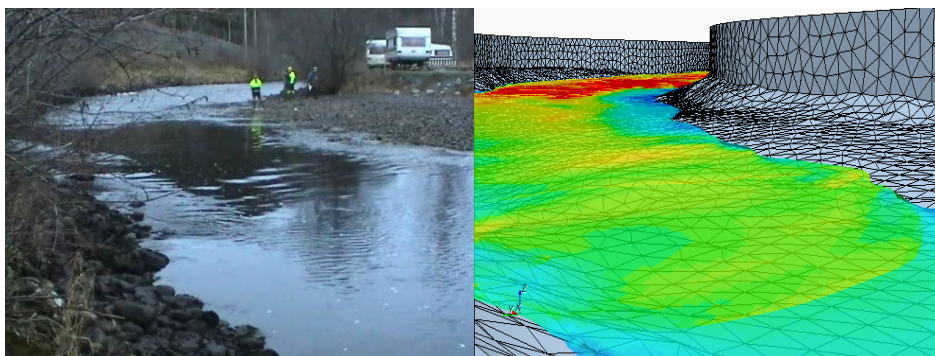
From the level of air mixing and disturbances seen on the water surface in the video, it is seen that the simulation resemble the transient velocity increase and water level rise fairly well at the times shown. Studying the attached videos will give a clearer idea of the resemblance. An observation is that the simulated water line rises and recedes before it rises again, resembling a wave hitting the shore. This effect is not observed in the field footage.

Figure 45 shows the surface velocity vector development from initiating the discharge rise at the inlet, and until the wave hits the outlet after 80 seconds. The flow field developed along the same pattern as seen in the steady state simulations, (figure 37) except that large eddies were generated close to the upstream bank, and just downstream of the bend. The Surface velocity vector video file shows that the eddies were created and dissipated before steady state flow was reached. At steady state no new eddies were created.

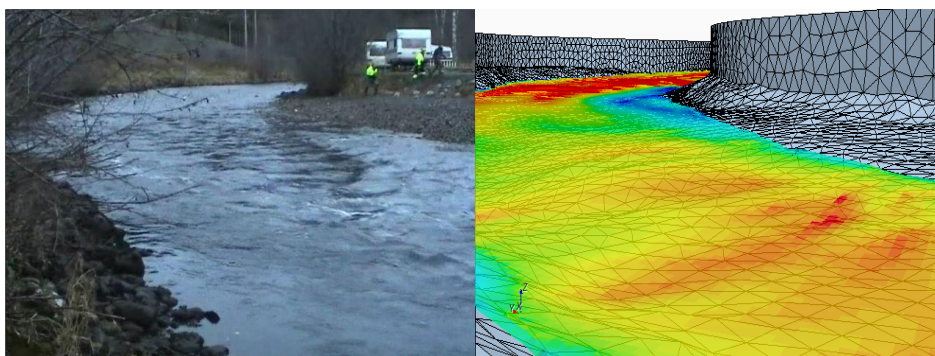
Unsteady flow. Comparison with video footage



a) After 45 seconds (0 seconds video time)



b) After 60 seconds (15 seconds video time)

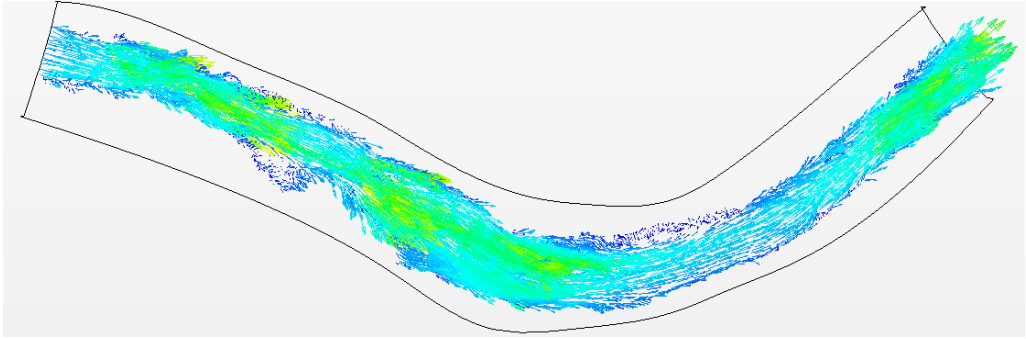


c) After 75 seconds (30 seconds video time)

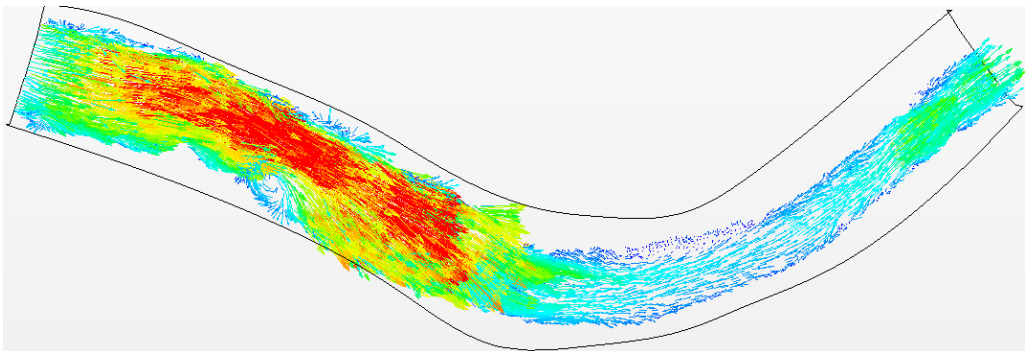


Figure 44: Comparison of simulations with video footage, unsteady flow, Lundesokna

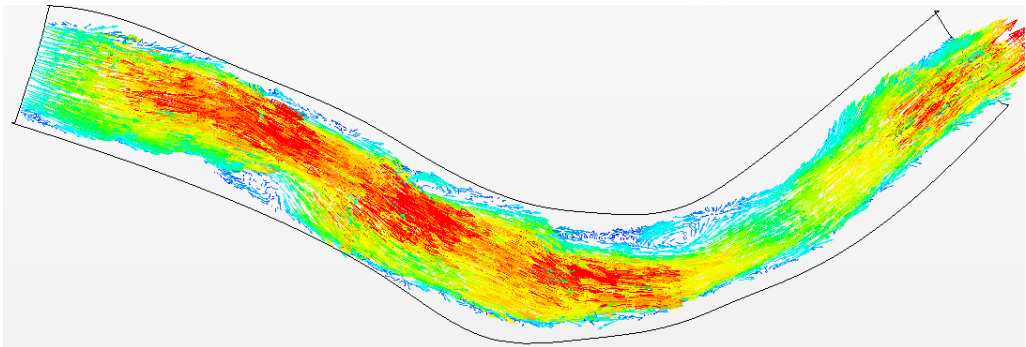
Unsteady simulation. Surface velocity vectors



a) At 0 seconds, $2 \text{ m}^3/\text{s}$ discharge steady state.



b) After 30 seconds



c) After 80 seconds, wave reaches outlet

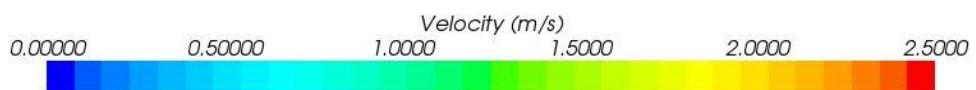


Figure 45: Surface velocity vectors [m/s], unsteady flow, Lundesokna

9 Discussion

9.1 Quality of the digital elevation models

A solid data basis is essential for getting good results in CFD. In particular the bathymetry data used for making the DEM is important. The data for the DEM were collected in different ways for the two models. For the Surna model, bathymetry data were collected by wading with a GPS-rover and by using an echo sounder, (section 6.4.1). Geometry data from the area surrounding the river were extracted from elevation curves. During the preliminary project, Pedersen (2012), the quality of the data were assessed by visualization in ArcGIS. The results are presented in Table 7.

Description of available geometry data			
<i>Date</i>	<i>Type</i>	<i>Measurement type</i>	<i>Quality description</i>
	Cross-sections	Differential GPS	Good
	Bed topography points	Differential GPS	Good
	Bed topography points	Echo sounder	Varies
	Points from elevation curves	Extracted from map	Varies
08.11.2011	Topography points at the right bank	Differential GPS	Good
24.11.2011	Topography points at the left bank	Differential GPS	Good

Table 7: Assessment of geometry data from Surna (Pedersen, 2012a)

The error margin for the differential GPS is within the range of a few centimeters, and measurements with a GPS-rover while wading can also be assumed to be in the range of about 1-2 centimeters. The data from the Echo-sounder is much less reliable, visualization of these data in ArcGIS showed that the data varies over a small area and is inconsistent with the GPS-rover data. Measurements by GPS-rover along the left bank were performed to validate the elevation curve data. These measurements showed large deviations between the elevation curves and GPS-rover measurements. A possible reason for this is that one or more recent landslides at the bank may have changed the geometry. This is assumed on the basis that the bank is steep and shows visual signs of movement. As the elevation curve data is only used at elevations higher than the river channel, i.e. at flood discharges, no further inquiries have been made to investigate the validity of the elevation curve data. The

elevation curve data is thus assumed to be unreliable. If the model is to be used for flood discharges it is recommended that this data should be reassessed.

Another important aspect of the geometry data is the spacing of the measured points. Figure 46 shows details of the spacing of different kinds of geometry measurements in Surna:

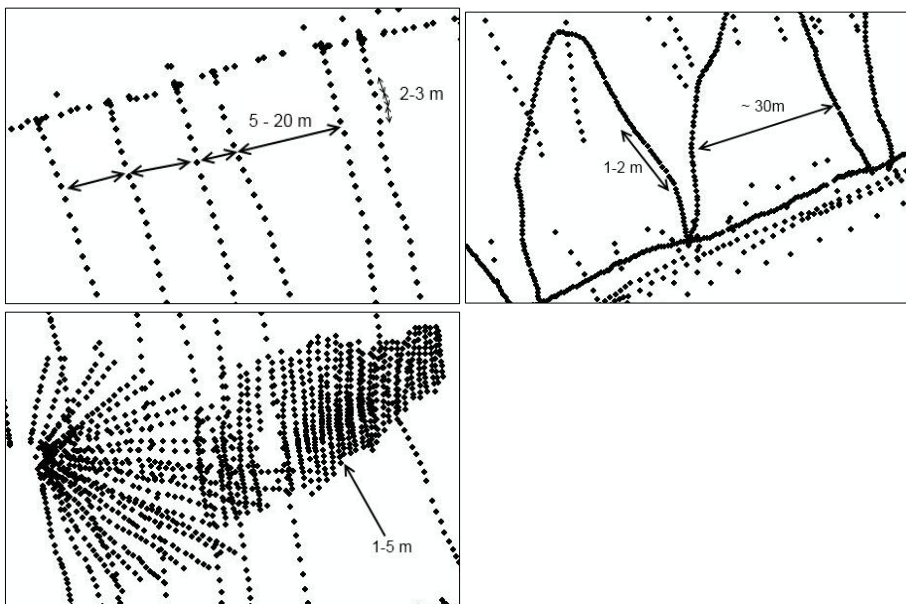


Figure 46: Spacing of geometry data in Surna. Top left: Spacing of cross sections, Top right: Spacing of echo sounder data, Bottom: Spacing in area close to island

As seen, the spacing varies for different part of the Surna bathymetry data basis. It is assumed that this spacing is good enough for modeling the big features of the riverbed, like the main chutes and position of the banks, while smaller details like bed form formations and large rocks etc. is not modeled. The roughness height parameter instead have to account for the friction caused by bed forms and particle distribution. In the deep upstream area where the echo-sounder was used, larger errors in the geometry can not be ruled out, both due to the large spacing of the measurements in the streamwise direction, and the relative uncertainty of the echo-sounder measurements.

The interpolation routines used for making a surface from the points is also equally important. The surface was made using interpolation routines available in SSIIM. The

interpolation routines is not suitable for interpolating points between cross-sections, as the points should have approximately equal spacing. To get a good surface, points were first added manually between cross-sections by linear interpolation. This is further described in Pedersen (2012a).

The data for Lundesokna was obtained using a TOPCON laser scanner (section 7.4.1). The laser scanned data has a spacing of between 0.04 and 0.4 meters. Some data were also collected by GPS-rover surveys, and this data has a spacing between 0.5 – 1.5 meters. The fine spacing allows for a detailed model, able to capture the bed forms and larger stones in the river. The roughness height parameter accounts for friction due to bed forms and individual stones at the bed. A model utilizing this detail level may thus not need to be modeled with a roughness height parameter. However, some details are lost in the export process from SSIIM, and the two Star CCM+ models uses 0.175 meter and 0.1 meter cell sizes at the bed. This means that while the data basis is good enough, these models due not utilize the potential, and a roughness height is still needed.

For models of natural rivers where high detail levels is needed, trying to model individual stones and bed forms could be an interesting prospect.

Large errors in the geometry of the Lundesokna models is unlikely due to the fine spacing used in the making of the DEM. The accuracy of the differential GPS and total station measurements should be within a few centimeters. The quality of Lundesokna DEM is thus considered to be good.

9.2 Grid generation

The generation of a suitable grid is essential for getting reliable results in CFD modeling. A key aspect of the grids made, both for Surna and for Lundesokna, were the balance between having a fine enough grid for getting accurate results, while keeping the computational time reasonable. The hardware available for this work has been regular high-end workstations (chapter 4). It would have been possible to use finer grids if the simulations had been run on a cluster. However, for engineering applications such clusters are not readily available, and an aspect of this thesis is to evaluate what can be done to make as efficient grids as possible.

9.2.1 *Star CCM+ versus SSIIM grid generators*

One of the most noteworthy differences between the SSIIM and Star CCM+ codes was how the grids were generated. In SSIIM it is possible to use an adaptive grid (section 3.2.3). This means that the grid has to be generated for every time step, but only cells that contain water is calculated. Star CCM+ generates an immobile grid, and uses a two phase flow model in which both cells containing water and air are calculated using the VOF method. SSIIM also has less restriction regarding the relative vertical to horizontal ratio of cells, and it is generally thus possible to have a larger quantity of cells in the vertical direction without making the cell count too high. The qualities of the SSIIM grid generator are good when dealing with free-surface simulations in natural rivers because the solutions in air-filled cells usually are uninteresting, and because the water depth usually is much smaller than the horizontal extent of the solution domain. This makes cells with large horizontal to vertical ratios an advantage for fully capturing a 3D flow. The advantages of the SSIIM grid-generator for the cases in this project are seen by comparing the cell size in the active solution domain (water filled cells) with the total cell count, as presented in table 8.

	SSIIM Grid	Star CCM+ Grid
Cell count	ca. 450,000 cells	605,769 cells
Horizontal cell extent	1 x 1 meters	1.4 x 1.4 meters
Vertical cell extent	Ca. 0.2 meters	0.7 meters

Table 8: Comparison of SSIIM and Star CCM+ grid data.

9.2.2 *Measures to reduce computational time in air-filled cells*

Since the solution in the air-filled cells was of no interest in this project, schemes to reduce the computational time in air cells have been attempted in Star CCM+. In particular inactive areas above the highest water level have been defined and a courser grid than in active areas were used here. The grid generation method is described in chapter 5. This method has successfully reduced the cell count in the

Surna Star CCM+ model from approximately 860,000 to 650,000 cells and in the Lundesokna model (m6) from approximately 1,600,000 to 850,000 cells. No tests has been conducted to assess possible errors due to the larger air cells; however the author considers it unlikely that the courser grid has any noteworthy influence on the solution in the active solution domain since the larger cells are kept clearly separated from water-filled areas. Only large air velocities will then influence the solution in the active domain. It should be noted however that the VOF model assumes equal velocities for air and water for cells containing both phases, see section 3.1.5. This means that care should be taken to avoid having the water surface touch the course grid, as this could cause large errors in water velocities at the water surface. For this purpose growth layers should be used in Star CCM+ (section 3.1.4).

9.3 Calibration of the roughness height parameter (k_s)

A dilemma that was encountered during the grid-generation phase of this project was a problem that seems to be particular for the modeling of natural rivers. The formulation of the friction at the bed in the wall laws used will give unphysical values if the roughness height (k_s) is larger than half the cell extent normal to the bed (CD-Adapco, 2011). On one hand it is important to have a fine grid close to the bed to get accurate results; on the other hand the roughness height parameter for natural rivers may be large. For the Surna simulation the roughness height was calculated to be 0.33 m by use of Van Rijn's empirical formula: $k_s = 3d_{90}$ (Van Rijn, 1984). Calibration in SSIIM later showed that a roughness height of 0.28 gave the closest matched water surface elevation to the measured values (section 7.6). While SSIIM allows for exceeding the recommended maximum roughness height of half the cell extent, this limit is automatically enforced in Star CCM+.

The Star CCM+ model had a vertical cell size of 0.7 meters near the bottom, while the roughness height was 0.28 m, so in this case no conflict was caused. For the Lundesokna model the roughness height was calibrated in Star CCM+ (section 7.6). The conclusion was that the best fit would be with a roughness height of 0.15 meters or higher. However, for the VOF method to work properly the water body should be covered by at least 2-3 cells (section 3.1.5). 30 cm vertical cells were assumed to be too coarse for resolving the water surface properly, therefore a roughness height of 8.75 cm and 17.5 cm cells were chosen as a compromise for the m6 grid.

It is shown in the results for the steady flow simulations (section 8.2.1 and 8.2.2) that the low roughness value causes a maximum under-prediction of the water-lines (horizontally) of 0.5 – 1 meter for 16.44 m³/s discharge. For the 10.58 and 20.63 m³/no under prediction of the water-lines are apparent. Given the horizontal cell size of 0.35 meters, an under-prediction in this range is expected. In conclusion the simulations do not seem sensitive to variations in the roughness height parameter in the range of 5-10 cm. The results from the calibration, however, show that the water line deviates much if the bed is modeled as smooth (section 7.6).

9.4 Results for Surna

9.4.1 Steady flow

In the preliminary project it was seen that SSIIM was able to simulate bed shear force development for a steady flow (Pedersen, 2012a). However little field data were available for validation of the results. The results presented section 8.1.1 show that the Star CCM+ model predicts similar flow fields and shear-force patterns to the SSIIM model. There were however some deviations in the magnitudes of velocities and shear-forces. The depth-averaged velocity plot (figure 35) show that the peak velocities deviate by 0.2 m/s. And the NRMSD is 17.74 %.

It is likely that these deviations at least partly are due to problems with unphysical velocities in cells close to the water surface. This is further explained below.

9.4.1.1 Problems with unphysical velocities

In figure 47 some areas where dots of high shear forces are shown in the Star CCM+ model are marked.

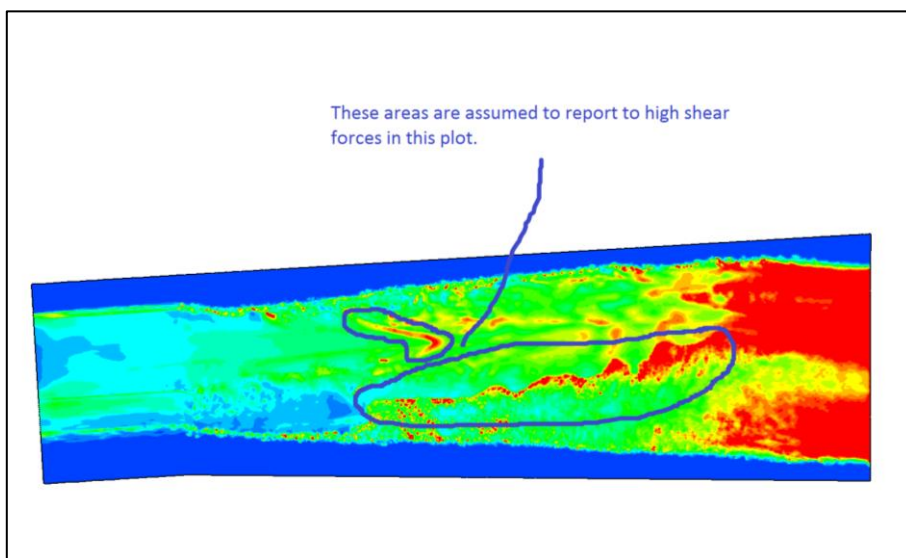


Figure 47: Errors due to unphysical velocities

A closer look on the Star CCM+ model reveals that the model clearly reports unphysical velocities in areas where the number of vertical cells covering the water depth is few. The problem is illustrated by comparing a cross section of Lundesokna, where the simulation shows good results, with a cross section from Surna (figure 48). Cells colored blue indicate water filled cells, and white cells only contain air. Red

cells contain a very small fraction of water. As seen in the top section, the water surface in Lundesokna was well defined for most of the computational domain, and the velocity vector field seems reasonable. Comparison to field measurements supports this (section 8.2.2). However, problems also occur here close to the banks where the number of vertical cells was few. In the bottom pictures velocity vectors with magnitude than 1 m/s are shown. The general velocity in the water was here about 0.5 m/s. Clearly these vectors represent unphysical velocities. The problem seems to occur in cells containing very small fractions of water (red cells).

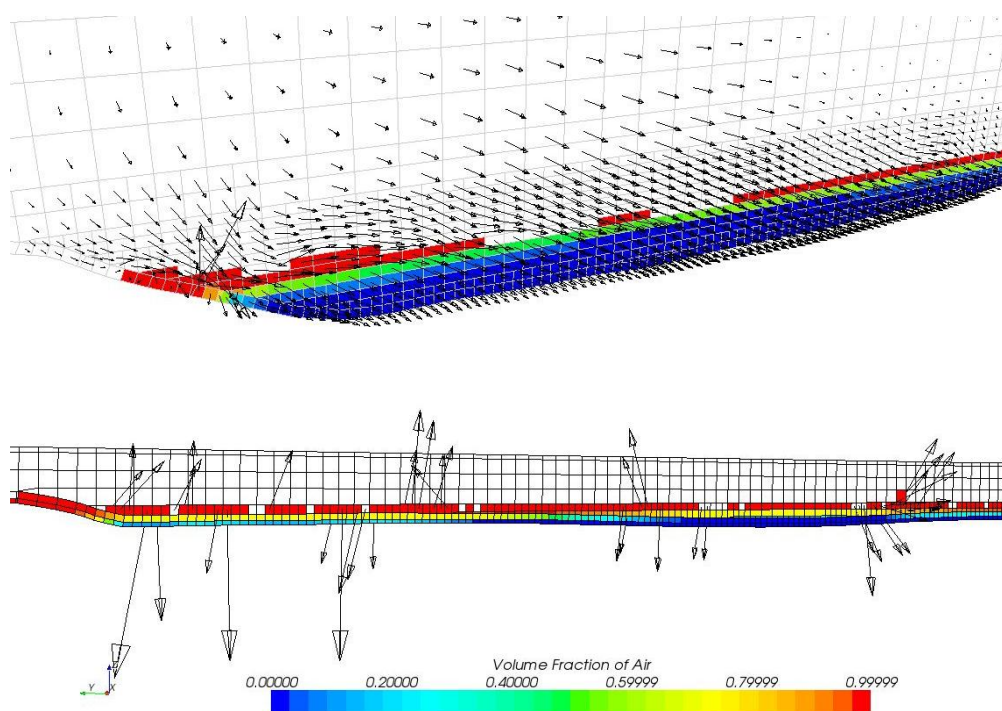


Figure 48: Velocity vectors and volume fraction of water in cross-sections. Top: Lundesokna, Bottom: Surna.

A possible cause of the problem was that too few cells were covering the depth of the water for the VOF fluid method to work properly. The Star CCM+ manual (CD-Adapco, 2011) recommends that at least three cells cover any body of water modeled to avoid problems with the VOF method.

The area close to the island downstream was as shallow as 30 cm and lower at 48.46 m^3/s discharge. This means that a vertical cell size of minimum 10 cm should be used

to model the river to have the recommended amount of vertical cells for the VOF method. As the hardware available for this thesis was insufficient to find solutions on a grid of this fineness within reasonable time, no attempt has been made to mitigate the problems described above.

It can be seen in figure 48 that cells with small fractions of water lays in the layer of cells that border the coarse part of the grid. Another possibility is that the large expansion ratio in these cells is causing the problem.

In light of the discussion above it seems likely that at least some of the differences in simulation results between SSIIM and Star CCM+ can be related to modeling inaccuracies due to the course Star CCM+ grid and problems with the VOF algorithms. However, as no other validation data is available, no conclusions can be made as to how much of the deviations are due to these problems.

9.4.2 Unsteady flow

The unsteady flow simulations presented in section 0 are discussed here.

The Star CCM+ model suffer from the same problems as for the steady flow simulations (section 9.4.1.1). The results support the observation made for steady flow that the general flow pattern to some extent was similar in the two models, while the velocity and shear-force magnitudes deviate. In addition the differences in boundary conditions can be clearly seen. Because of the quasi unsteady approach in SSIIM the discharge has to be equal at the inlet and outlet at all time-steps. SSIIM is then unable to capture the effects of the wave traveling through the model. This means that the SSIIM simulation is not fully transient.

A question that arises here is how much the limitation in wave simulation in SSIIM influences key data such as the peak shear-force and velocities in the model. The current study is unable to answer this question as the steady flow results also show large deviations between the two models. It is however an interesting theme for further study.

The results (section 0) show that peak forces at the outlet are about 10 minutes delayed in Star CCM+ compared to SSIIM. This corresponds to an average velocity 0.8 m/s for the wave traveling from inlet to outlet. When accounting for the difference due to the wave traveling through the model the two models show comparable shear-force patterns but deviating magnitudes as for the steady flow conditions.

9.4.3 Validation

The available velocity measurements from the site are not of good enough quality to be used for validation of the SSIIM and Star CCM+ models. As no other data is available for validation, the only way to validate the models was to compare them to each other. It was difficult to directly compare the models due to the problems with a coarse Star CCM+ grid described in section 9.4.1.1 and the limitations in capturing transient flow in SSIIM (section 9.4.2).

However, as observed in the discussions, both for steady and unsteady flow (section 9.4.1 and 9.4.2) the SSIIM and Star CCM+ models seem to predict comparable general flow and shear-force patterns, while the magnitude deviates. To sum up it seems that the Star CCM+ simulations support the general flow pattern results of the SSIIM model, but were unable to give any good validation of the magnitudes of velocities and shear forces

9.5 Results for Lundesokna

9.5.1 Steady flow

Steady flow simulations were run for discharges between 2-20 m³/s.

Water lines for discharges between 10-20 m³/s and velocity measurements in a cross-section for 20 m³/s were used to validate the model (section 8.2.2). The water lines were generally predicted within 0.5 – 1 meter average error. The RMDS for the depth averaged velocities is 0.13 m/s, and the NRMDS 9%. This means that the model was able to capture the velocities at 20 m³/s discharges with an average 9% deviation compared to the velocity range. The peak was captured with a difference of about 0.05 m/s.

These results indicate that the model was able to predict the flow field and water lines for discharges between 10-20 m³/s with good accuracy.

Steady state solutions at 2 and 20³/s for the m7 grid were used to investigate the grid sensitivity of the m6 grid for steady flow (section 8.2.2.1). The presented figures show that the changes in the surface velocity vectors were minor. Changes in water depth were also investigated, and found to be equally small. It is therefore concluded that the steady flow results presented in section 8.2.1 was not highly grid dependent.

9.5.2 Unsteady flow

While calibration and validation data were available for the Steady flow simulations, similar measurements do not exist for the unsteady flow conditions. The only means of validation available is the video footage. Comparing the simulated data with the video visually shows that the simulation and the video match to some extent.

Looking at the amount of disturbance at the water surface it can be seen that the velocity increases in a similar fashion to that in the simulation. Also indications that the water just upstream of the bend was flowing with a high velocity can be seen in the video, as the water turns white due to air entrainment. This together with the good results from the steady flow simulations indicates that the unsteady simulation captures the transient flow to some extent. Field data measurements for transient conditions are, however, needed to quantify the accuracy of the simulation.

A particular difficulty with modeling the unsteady simulation compared to the steady simulations was that the transient boundary conditions are not well known or defined. At the velocity inlet it was assumed that the change in discharge happens instantaneously (section 7.8). In reality the rate of change is not known, but may be in the range of 5-20 seconds given the acceleration time of the upstream turbine and the water rise shown in the video footage. Also, the transient pressure conditions at the downstream boundary are not known. The conditions at the downstream boundary will influence the water surface level further upstream when the flow is subcritical upstream of the boundary. More accurate conditions for the upstream and downstream boundary could be obtained by measuring the water level continuously during a hydro peaking event. This could be done using pressure loggers with a sampling rate of 5-10 seconds.

An observation made was that the water-line simulated in Star CCM+ rises, recedes and then starts rising again. This seems to resemble a wave hitting the shore. The observation is not observed in the video footage. A possibility is that the instantaneous change in discharge at the inlet causes a larger wave than for the field case, inducing more prominent wave effects. Doing the simulation with a linearly increasing discharge during 5-20 seconds at the inlet might be an interesting prospect. This could unfortunately not be carried out within the time-frame of this thesis.

Currently there exist plans in connection with the EnviPEAK project to collect field data that will allow validation of the unsteady simulation. A special balloon will be used to be able to film the river from above. Several points in the surrounding geometry will then be georeferenced from the video to be able to compare the water surface rise to the simulation.

9.6 The width to depth ratio

As shown in section 9.4 and 9.5 Star CCM+ was able to get good results for Lundesokna, while the simulations in Surna were less successful. Partly this can be seen in connection with the larger width to depth ratio of Surna. The fact that the VOF method requires 2-3 cells or more over the depth of the water makes the VOF method less ideal for rivers with large width to depth ratios because there will likely be large areas where only one or two cells over the depth would otherwise be ideal. An interesting prospect is therefore to look at the width to depth ratios for rivers to determine whether the river practically can be modeled with Star CCM+ given the available computational resources.

In SSIIM this is no problem as the adaptive grid can handle single cells over the depth.

10 Conclusion

The objective of this thesis has been to investigate the possibilities for modeling unsteady hydro-peaking scenarios in Norwegian regulated rivers by means of computational fluid dynamics. In particular the capabilities of the two numerical simulation software packages Star CCM+ and SSIIM have been investigated. The focus has been on Star CCM+.

Two rivers have been modeled. In Surna a Star CCM+ model was developed for running steady and unsteady free-surface simulations. The steady simulation results were compared to results in a SSIIM model developed by Pedersen (2012a) during a project preceding this thesis. The unsteady flow simulation was compared to unsteady flow simulations run on a further developed version of the SSIIM model. In Lundesokna a Star CCM+ model was developed for steady and unsteady flow and compared with measured data from the site.

A hypothetical hydro-peaking scenario was developed for Surna based on data for a similar river. For Lundesokna the model was based on a full-scale hydro-peaking experiment.

The models have been developed from 3D surfaces to fully operational numerical models for running steady and unsteady simulations. Extensive grid experimentation has been utilized to optimize the grid making process for natural rivers. An optimized grid generation method for free-surface grids in natural rivers using the VOF method in Star CCM+ was developed during this process. The possibilities for calibrating the roughness height parameter in the model have been investigated. Here a conflict between the often high roughness heights in natural rivers and the way the wall-laws are implemented was identified. Implications of this problem and how to deal with it were discussed. A physical model setup was developed based on theory on 3D CFD modeling. Initial conditions and boundary conditions were set up based on theory and experimentation. Problems regarding the available data for boundary conditions during unsteady simulations were identified and discussed, and assumptions for the boundary conditions were made where necessary.

The main conclusions are:

- *Star CCM+ is able to predict steady state flow fields and water surface elevation in natural rivers with good accuracy, and show promise in modeling unsteady conditions. However, for rivers with a high width to depth ratio the need for computational resources is high.*
- *SSIIM is able to model Steady flow and quasi-unsteady flow conditions in natural rivers. The adaptive grid method used in SSIIM requires far less computational power than for Star CCM+ for modeling free-surface flow.*

Conclusions from the modeling process were:

- The adaptive grid in SSIIM gives lower cell-counts than the VOF method in Star CCM+ for free surface flow.
- The cell count in Star CCM+ can be reduced drastically by using refinements in water-filled areas.
- The way wall-laws are implemented limits the size of the roughness height parameter in Star CCM+. The results suggest that the solution is not very sensitive to small changes in roughness.

The results from the simulations showed that:

- The developed SSIIM model is able to successfully simulate bed shear-forces for steady and unsteady flow. Due to limitations in SSIIM transient wave effects cannot be fully captured.
- The developed Star CCM+ model was only partially successful in modeling Surna due to errors in the solution. A review of the model suggests that the problems are due to the coarse grid.
- The Star CCM+ model predicts a similar flow and shear-force pattern to SSIIM, but magnitudes deviate.
- The Lundesokna model was able to predict measured water-lines between 10 and 20 m³/s discharge and velocities at 20 m³/s with high accuracy at steady flow conditions.
- For unsteady flow conditions the simulation results seem to resemble the video footage well. The video footage is however not of sufficient accuracy to quantify the accuracy of the solution.

10.1 Recommendations for further work

After this thesis, the most important immediate further work to be done is the collection of field-data that can quantify the accuracy of the unsteady simulation in Lundesokna. As mentioned plans to do this exist within the EnviPEAK project. What should be collected are primarily points at the water line for a hydro-peaking event. High-resolution (5-10 second sampling rate) pressure-logger data at the model inlet and outlet could also be collected during the event to avoid having to calibrate the boundary conditions.

Another important theme that came up in the discussion is the influence of unsteady effects on key-data like shear-forces, flow fields and water surface elevations. Work should be done to clarify when fully unsteady simulations are necessary for impact-assessment applications, and when steady state simulations are sufficient.

Further, it is recommended that the CFD-methods described in this thesis are applied to more rivers, to quantify the practicality and accuracy of the methods.

11 Bibliography

- Blazec, J. (2005). *Computational fluid dynamics: Principles and applications, second ed.* London: Elsevier.
- CD-Adapco. (2011). *User Guide, Star CCM+ Version 6.06.011.* CD-Adapco.
- Fischer-Antze, T., Olsen, N., & Gutknecht, D. (2008). Three-dimensional CFD modeling of morphological bed changes in the Danube river. *Water Resources Research, VOL 44.*
- Flow Science. (n.d.). *Simulating fluid Flows with Free Surfaces.* Retrieved 05 11, 2012, from Flow3D.com/cfd-101: <http://www.flow3d.com/cfd-101/cfd-101-free-surface-fluid-flow.html>
- Halleaker, J. H., Sundt, H., Alfredsen, K. T., & Dangelmaier, G. (2007). Application of Multiscale Environmental Flow Methodologies as Tools for Optimized Management of a Norwegian Regulated National Salmon Watercourse. *River Research and applications 23*, 493-510.
- Halleaker, J., Alfredsen, K., Arnekleiv, J., Fjelstad, H., Harby, A., & Saltveit, S. (1999). Environmental Impacts of Hydro Peaking - With Emphasis on River Nidelva in Trondheim, Norway. *Optimum use of run-of-river hydropower schemes.* Trondheim.
- Hasaas, Å. (2011). *Feltnmåling av strømningsforhold i inntaksmagsin til kraftverk.* Trondheim: Department of Hydraulic and Environmental engineering, NTNU.
- Haun, S., & Olsen, N. (2012). Three-dimensional numerical modelling of the flushing process of the Kali Gandaki hydropower reservoir. *Lakes & Reservoirs: Research and Management 17*, 25-33.
- Hirt, C., & Nichols, B. (1981). Volume of Fluid (VOF) Method for the Dynamics of Free Boundaries. *Journal of computational physics 39*, 201-225.
- Labiod, C., Godillot, R., & Caussade, B. (2007). The relationship between stream periphyton dynamics and near-bed turbulence in rough open-channel flow. *Ecological modelling Volume 209, Issues 2-4*, 78-96.
- Mulet-Casas, R. (2012, 06 02). Personal contact. Trondheim.

- Murthy, J. Y. (2002). *Numerical Methods in Heat, Mass and Momentum Transfer (draft notes)*. School of Mechanical Engineering, Purdue University.
- Olsen, N. (2011a). *A three-dimensional numerical model for Simulation of Sediment movements In water Intakes with Multiblock option - User's manual*. Trondheim: NTNU.
- Olsen, N. (2011b). *Numerical modelling and Hydraulics*. Trondheim: The Norwegian University of Science and Technology.
- Olsen, N., & Haun, S. (2010). Free surface algorithms for 3D numerical modelling of reservoir flushing. *RiwerFlow 2010*. Braunschweig, Germany.
- Patankar, S. V. (1980). *Numerical heat transfer and fluid flow*. London: Taylor & Francis.
- Pedersen, Ø. (2012a). *Three-dimensional numerical modelling of the Surna river*. Trondheim: Department of Hydraulic and Environmental Engineering, NTNU (The document is provided as a digital attachment).
- Pedersen, Ø., & Rütther, N. (2012b). Modeling bed shear stress on an armored river bed due to hydropower peaking. (The document is provided as a digital attachment).
- Rodi, W. (1980). *Turbulence models and their applications in hydraulics*. Rotterdam, The Netherlands: Balkema A. A.
- Rütther, N., Jakobsen, J., Olsen, N., & Vatne, G. (2010). Prediction of three dimensional flow field and bed shear stress in a regulated river in Mid-Norway. *Hydrology research*, 41.2, 145-152.
- Schlichting, H. (1979). *Boundary layer theory*. New York: McGraw-Hill.
- Shih, T., Liou, W., Shabbir, A., Yang, Z., & Zhu, J. (1994). A New k-epsilon Eddy Viscosity Model for High Reynolds Number Turbulent Flows - Model Development and Validation. *NASA TM 106721*.
- Spiller, S., Rütther, N., Belete, K., & Strellis, B. (2011). Assessing environmental effects of hydropower peaking by 3D numerical modeling. *Annual conference on hydraulic engineering, 34th proc*. Dresden: Technical University.
- Store Norske Leksikon. (2009, 11 26). *Lundesokna*. Retrieved 04 18, 2012, from Snl.no: <http://snl.no/Lundesokna>

- Tesaker, E., Fergus, T., Einar, L., & Bargel, T. (2010). 5. Erosjon, massetransport og skred. In T. Fergus, K. A. Hoseth, & E. Sæterbø, *Vassdragshåndboka* (pp. 149-235). Trondheim: Norwegian University of Technology and Science.
- Van Rijn, L. (1984). Sediment transport: Bed load transport. *Journal of hydraulic engineering - ASCE issue 10*, 1431-1456.
- Weiming, W., Rodi, W., & Wenka, T. (2000). 3D Numerical Modeling of Flow and Sediment Transport in Open Channels. *J. Hydraul. Eng.* 126(1), 4-15.

12 Appendixes

Appendix A: List of digital attachments

Hydro-peaking event video footage

Hydropeak_Video.wmv: This file contains the video footage for the hydro-peaking event. (section 7.4.4) The video was used for setting up the models in Lundesokna, and for comparison with the unsteady results (below).

Lundesokna unsteady results

These videos are part of the results from the unsteady simulations for Lundesokna, presented in section 8.2.3.

M06_Video_Timed.avi: A scene from the same point of view as the Hydro-Peaking event video. Velocity magnitudes are plotted on the water surface. A plot was exported every 0.1 second physical time from Star CCM+. The video is timed to fit the Hydro-peaking event footage. The simulation is run from 770 – 890 seconds on the m6 grid.

M07_Video_Timed.avi: Same as for M06_Video_Timed, but on the m7 grid. Note the different scale. The video is run from 765 – 780 seconds. The different timing from the m6 video is because this seemed to give a better fit with the hydro-peaking footage.

M07_Surface_velocity_vectors.avi: Plotted velocity vectors on the VOF free water surface from 720 seconds to 900 seconds.

M07_WaterDepth.avi: Plotted water depth from 720 to 900 seconds. The water depth is calculated by the static pressure at the bed.

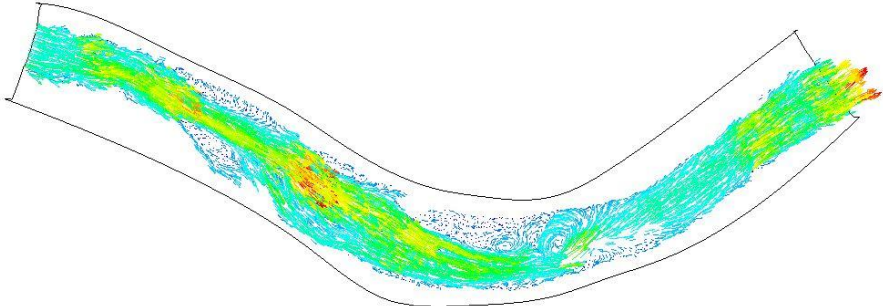
Documents

Pedersen Ø. (2012) – Three-dimensional modeling of the river Surna.pdf: This document describes the data basis, modeling and steady simulation for the Surna SSIIM model.

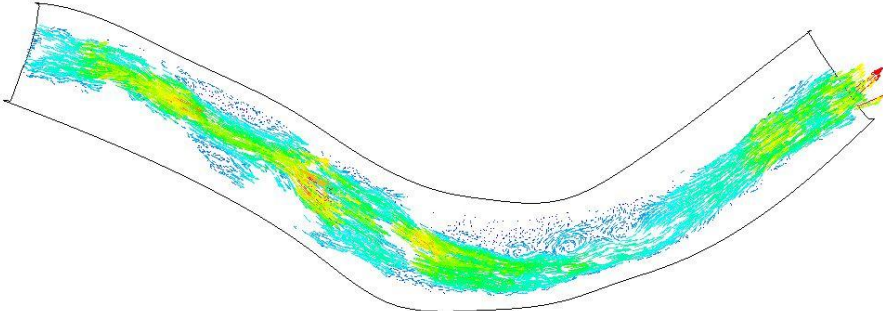
Pedersen, Ø. & Rütther, N. (2012) - Modeling bed shear stress on an armored river bed due to hydropower peaking.pdf: This paper was written for the IAHR-APD 2012 conference in Korea. It is not part of this thesis, but is provided here for your consideration.

Appendix B: Grid sensitivity tests in Lundesokna

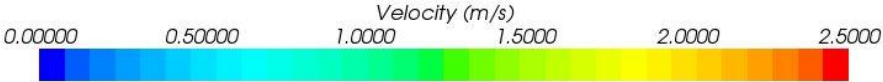
Surface velocity vectors [m/s]:

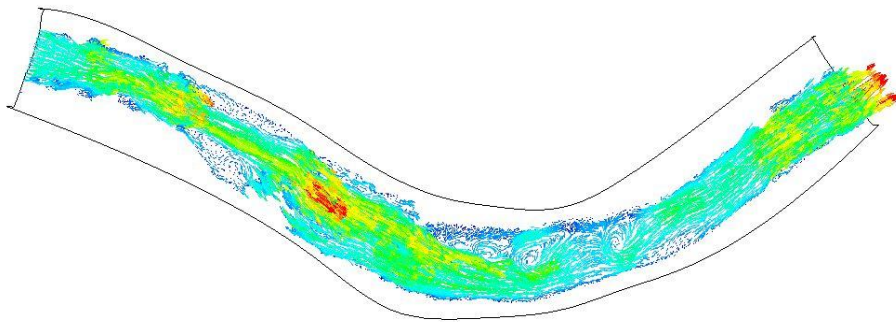


a) m1

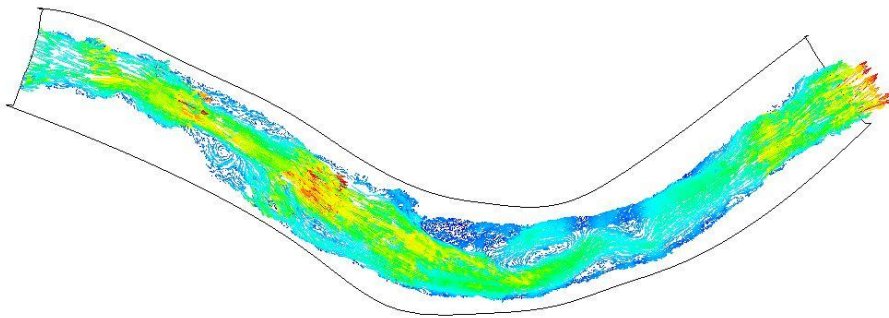


b) m2

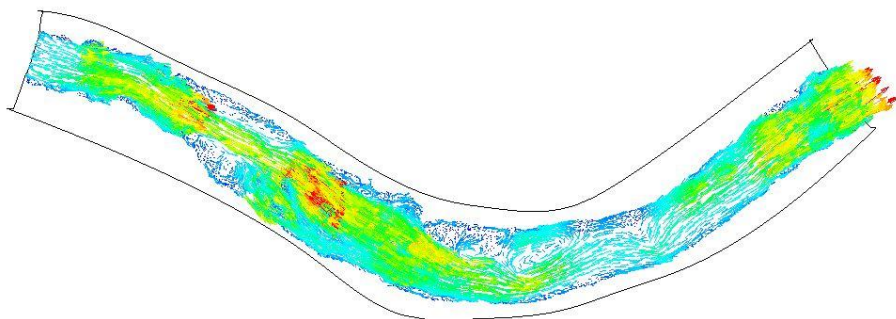




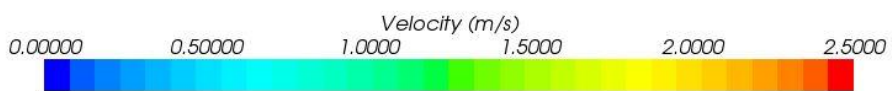
c) m3



d) m4



e) m5



Appendix C: Map of the sites

